DNA DOUBLE-STRAND BREAK REPAIR DEFICIENCY IS ASSOCIATED WITH CHANGES IN CELL CYCLING AND CELL MORPHOLOGY IN *SACCHAROMYCES CEREVISIAE*

by

Monica F. Weis, B.S.

A thesis submitted to the Graduate Council of
Texas State University in partial fulfillment
of the requirements for the degree of
Master of Science
with a Major in Biochemistry
May 2017

Committee Members:

L. Kevin Lewis, Chair

Karen Lewis

Liqin Du

FAIR USE AND AUTHOR'S PERMISSION STATEMENT

Fair Use

Duplication Permission

ACKNOWLEDGEMENTS

First and foremost, I would like to thank Dr. Kevin Lewis for being such a dedicated advisor. His patience and kindness is unmatched by anyone I have met. He commits his time and advocates for all students like they are his only student. My heartfelt thanks.

My completion of this project would not have been possible without the supportive and caring lab-mates I was surrounded with and the positive atmosphere we created to work in. I have never known friends like you and I hope our friendships last a lifetime.

Finally, to all of my loving and supporting family. Granny, your letters and kind words brightened my toughest days. Mom, for just listening to me when I needed it. Mike, for accommodating my crazy schedule and for your consistency when I need you. I am so grateful to have you all in my life.

TABLE OF CONTENTS

Page

LIST OF TABLES

Table **Page**

LIST OF FIGURES

Figure **Page**

I. INTRODUCTION

Self-assembly using deoxyribonucleic acid (DNA) as a blueprint is ubiquitous in living systems. DNA is a polymer and the sequence of nucleotide monomers act as a code that regulates the expression of genes encoding proteins and functional RNAs in a cell. Nucleic acid monomers form a chain via phosphodiester bonds. The chains associate with each other to form a double helical structure with two deoxyribose phosphate backbones. Guanine, adenine, thymine, and cytosine bases vary on the backbones and form the actual code. Two complementary DNA strands arranged in opposite directions form the double helical structure held together by hydrogen bonding between bases on opposite strands and planar stacking between adjacent bases. Guanine base pairs with cytosine and adenine base pairs with thymine. The base pairs are strong enough to hold the molecules together in optimal biological conditions, yet can easily denature to enable transcription and replication. DNA and its encoded sequence are the instruction manual critical for all lifeforms to carry out the most basic of functions. Thus, it is crucial that chromosomal structure and sequence are conserved (1).

The genomic integrity of an organism is constantly being challenged. Chromosomal DNA lesions are continuously being introduced by both intracellular

metabolic processes and extracellular agents. It is estimated that a single human cell experiences ~ 50,000 - 80,000 DNA lesions per day that must be repaired (4). Exogenous sources that can introduce DNA insults include radiation and exposure to clastogenic (DNA strand breaking) chemicals, and endogenous sources include enzymes and the reactive oxygen species that are a natural consequence of aerobic metabolism (1-4).

Sources of exogenous DNA damage

Solar radiation is radiant energy emitted by the sun. Some of this energy is emitted in invisible rays called ultraviolet (UV) radiation and damages DNA by the absorption of photons. The predominant genotoxic photoproducts of UV radiation are dimers between adjacent pyrimidine bases, called cyclobutane pyrimidine dimers (CPDs) and 6,4-photoproducts (4).

Ionizing radiation is any electromagnetic wave or particle that can remove an electron from an atom or molecule in the medium through which it travels. When living material is ionized, it temporarily excites molecules into reactive species that are capable of causing direct DNA damage or indirect DNA damage through the generation of reactive oxygen species (ROS) (4).

DNA damage can also be chemically introduced by clastogenic chemicals such as bleomycin or methyl methanesulfonate (MMS). MMS is an alkylating agent that methylates the nitrogen and oxygen atoms in DNA bases as well as phosphodiester bonds. This can lead to secondary DNA damage due to stalled and unresolved replication forks upon encountering methylated bases (10). The toxicity of bleomycin, a chemotherapeutic glycopeptide antibiotic, rests primarily in the generation of single-

strand and double-strand DNA breaks. The exact mechanism of action is unknown although it is thought that bleomycin acts as a pseudo-enzyme that, upon chelation of Fe^{2+}, generates free radicals in the presence of O_2 (Fenton reaction) (5).

Higher level eukaryotic aerobic organisms cannot live without oxygen, yet it is inherently a threat to their existence due to the two valent electrons present in its molecular form. The superoxide anion radical, hydrogen peroxide and the extremely reactive hydroxyl radical are common products resulting from reduction of molecular oxygen to water during mitochondrial respiration. This is thought to be the primary source of intracellularly generated ROS, providing the basis for the so-called "oxygen paradox" (5): oxygen is required for survival yet is inherently detrimental.

Although each DNA damaging agent has a signature type of damage that it creates, some DNA damage types do not have mutually exclusive sources since secondary lesions commonly occur from different types of original damage sites. Secondary lesions that can occur within the chromosome include damaged bases, sugar alterations, abasic sites (AP sites), DNA-protein crosslinks, and single-strand or double-strand breaks (DSBs) (1,5).

Repair processes for DNA damage in living systems

Repair processes for the plethora of inevitable DNA lesions that occur have been found among cellular organisms investigated indicating that DNA damage is a ubiquitous threat to the conservation of the genetic code. Pathways that have been characterized include base excision repair (BER) for the repair of damaged bases or abasic sites, nucleotide excision repair (NER) for the removal of bulky lesions such as ultraviolet

light-induced pyrimidine dimers, and mismatch repair (MMR), which removes misincorporated bases that occur during replication and recombination. In response to double-stranded breaks two major pathways are used: nonhomologous end-joining (NHEJ) and homologous recombination (HR) (also called homology-directed repair or HDR) (2,4).

Pathways for the repair of double-stranded breaks

NHEJ is the simpler of the two pathways, involving the direct ligation of the broken chromosome ends (Figure 1). Minimal energy expenditure is required, but it is also associated with information loss at the break sites (2, 4). There are at least 8 genes whose products form three essential protein complexes to carry out NHEJ in cells of the budding yeast *Saccharomyces cerevisiae*: Yku70/Yku80, Mrx, and DNA Ligase IV. The Yku70/Yku80 complex is a key player in the initiation of the NHEJ repair pathway and is involved in binding the ends of broken chromosomes as a heterodimeric ring comprised of Yku70 and Yku80 to initiate NHEJ and recruit further complexes. It is thought that the complex also serves to protect damaged and exposed DNA ends from nucleases. The Mrx complex, comprised of Mre11, Rad50, and Xrs2, bridges the two ends of the broken chromosome, ensuring that they remain in close proximity for repair, as well as recruiting the DNA Ligase IV complex. In humans, Xrs2 is replaced with Nbs1. The Mre11 portion of this complex has a 3'-5' double-stranded DNA exonuclease activity in the presence of manganese as well as single-stranded endonuclease and weak helicase activities (6). The Rad50 subunit of Mrx has ATP-binding activity as well as possible adenylate kinase activity (7) and it has been suggested that the Xrs2 subunit interacts with the DNA Ligase IV complex to facilitate ligation of the two DNA strands (6). The DNA Ligase IV

complex, consisting of Dnl4, Lif1, and Nej1, completes the repair process. The Dnl4 subunit of the DNA Ligase IV complex is a DNA ligase that is ATP-dependent (2) and the Lif1 subunit is suggested to associate with the Xrs2 subunit in Mrx (6, 8, 38). Of the three protein complexes involved in NHEJ, Mrx is unique because it is involved in the HR pathway as well. NHEJ is the secondary pathway for the repair of DSBs in *Saccharomyces cerevisiae* (budding yeast) but the primary pathway in humans (2, 5).

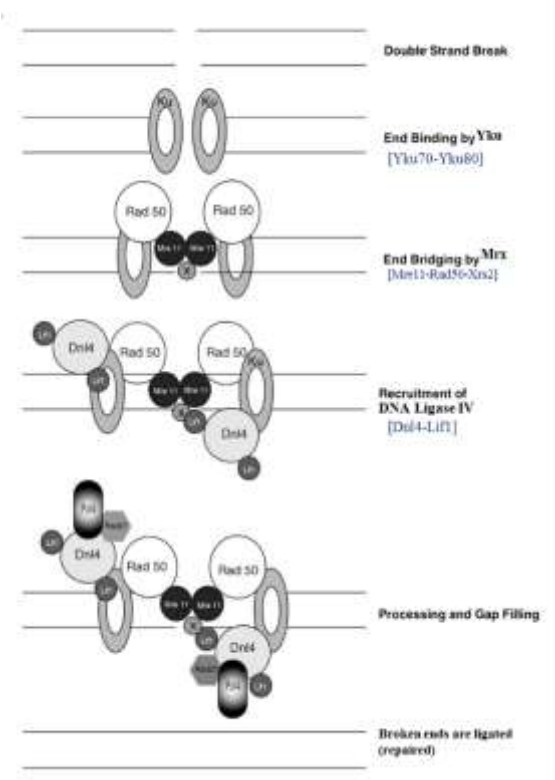

Figure 1. Schematic representation of the nonhomologous end-joining pathway for the repair of DNA double-strand breaks (8).

HR is considered the more conservative of the two pathways for DSB repair because it uses homologous DNA regions as a template to repair the break and is highly accurate (Figure 2). Major genes involved with HR in yeast include *RAD50, RAD51, RAD52, RAD54, RAD55, RAD57, RAD59, RDH54, MRE11,* and *XRS2,* which are all

members of the RAD52 group of repair genes (11, 12). The protein products of these genes perform an intricate, multistep process that involves two known complexes, Mrx (discussed above) and the Rad52 complex (comprised of Rad51-Rad52-Rad54-Rad55-Rad57-Rad59) (9, 10). The Mrx complex nuclease, in conjunction with other nucleases, creates long 3' single-stranded overhangs that are hundreds of nucleotides long on both broken DNA strands (Figure 2). This resection by Mrx takes place in HR but not NHEJ and is regulated by cell cycle phase and by specific proteins such as Rif1 (37). Resection is followed by binding of the single-stranded DNA binding protein complex, Replication Protein A (Rpa), which protects the exposed DNA strands. Rpa recruits the Rad52 complex of proteins for homology searches, strand invasion and information exchange with an unbroken homologous chromosome. This process is concluded with DNA replication, branch migration, nucleosome assembly, and resolution resulting in a repaired chromosome. Additional protein complexes are also recruited during this process, such as those required for DNA damage checkpoint responses, nucleosome remodeling, sister chromatid cohesion and other processes (3, 31). Although many specifics of the HR mechanism remain unknown, functions of several of the proteins involved have been characterized. Rad51 is a strand exchange protein that forms a helical filament with long 3'ssDNA ends that searches for sequences with homology to the broken DNA ends. Rad52 helps to stimulate strand exchange and facilitates Rad51 binding to ssDNA by displacing the single-stranded DNA binding protein Rpa. The Rad52 protein has been shown to be most critical, as *rad52* mutants often display more severe phenotypes than *rad51, rad54* or other mutants in the Rad52 group in many assays (4, 11). The homologous recombination pathway is unable to be utilized in *rad52*

mutants (9). Rad54 is a DNA-dependent ATPase that stimulates strand exchange by modifying the topology of homologous dsDNA strands. Rad55 and Rad57 help to stabilize the binding of Rad51 to ssDNA. The role of Rad59 is unclear and *rad59* mutants have very modest phenotypes, although the Rad59 protein has sequence homology to Rad52 (32). HR is the primary pathway for the repair of double-stranded breaks in yeast but the secondary pathway in humans (4, 6).

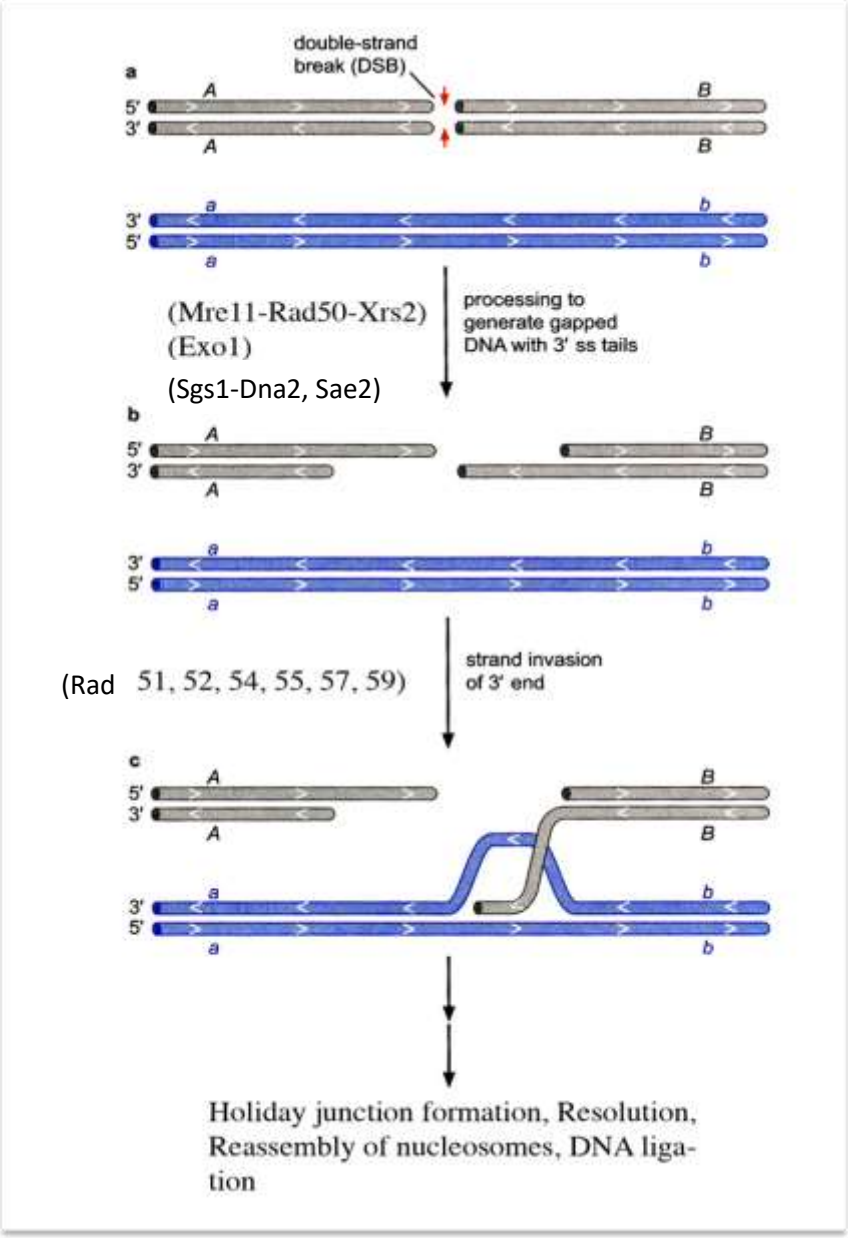

Figure 2. Schematic representation of the homologous recombination pathway for the repair of DNA double-strand breaks. Adapted from (34).

The reason for preferential use of NHEJ by human cells is likely to be the substantial amount of repetitive DNA in multicellular eukaryotes (2). Except after DNA replication when sister chromatids are close (late S phase and G_2 phase) the search for homologous sequences in the chromosomes during HR would more than likely lead to

high levels of genetic exchange between repetitive elements, possibly leading to chromosomal translocations or deletions. For example, a break in an Alu repeat (a repetitive DNA sequence) has almost one million possible donors (14). Therefore, organisms with a highly repetitive genome may favor NHEJ, as a small deletion associated with NHEJ is less mutagenic than frequent aberrant recombination events. The small deletion events may also be better tolerated in higher organisms.

Yku proteins are important for both NHEJ and telomere stability

Telomeres are repetitive sequences found at the ends of linear eukaryotic chromosomes that are essential for protecting the genome from being compromised due to degradation by nucleases, end-to-end fusions, or recombination events during each cell division. They also solve the end replication problem, whereby every time the chromosome replicates a portion of the lagging strand cannot be replicated and is thus lost. In wildtype *S. cerevisiae*, telomeres are from 350-500 bp in length. Ku plays several roles at the telomere regions that are important for maintaining genomic stability including regulating telomere DNA replication, transcriptional silencing of telomere-proximal genes, and nuclear positioning of telomeres. Ku also protects telomeres from recombination or chromosomal end-joining as well as nucleolytic degradation (42).

The cell cycle regulates important cellular functions

Faithful replication and propagation of genetic information is paramount for cell viability. Therefore cells have evolved complex regulatory systems to coordinate the order and timing of cell cycle events to allow for complete and accurate DNA replication (Figure 3). The eukaryotic cell cycle is divided into four phases, G_1, S, G_2, and M. G_1 is

the main growth phase, S phase is when DNA replication occurs, G_2 is when the cell prepares for mitosis, and M is mitosis, where chromosome segregation, nuclear division, and cytokinesis occur. The two "G" phases, or gap phases, provide time for growth and for the cell to monitor the internal and external environment to ensure it is adequately prepared to commit to chromosomal replication or cell division. When levels of radiation or chemically induced lesions are high, DNA damage-responsive cell cycle checkpoints are activated, causing cells to pause in the G_2 phase of the cell cycle. This arrest is the result of the DNA Damage Response (DDR) which provides time for repair of damaged DNA and prevents the passage of erroneous coding information to subsequent cells (4).

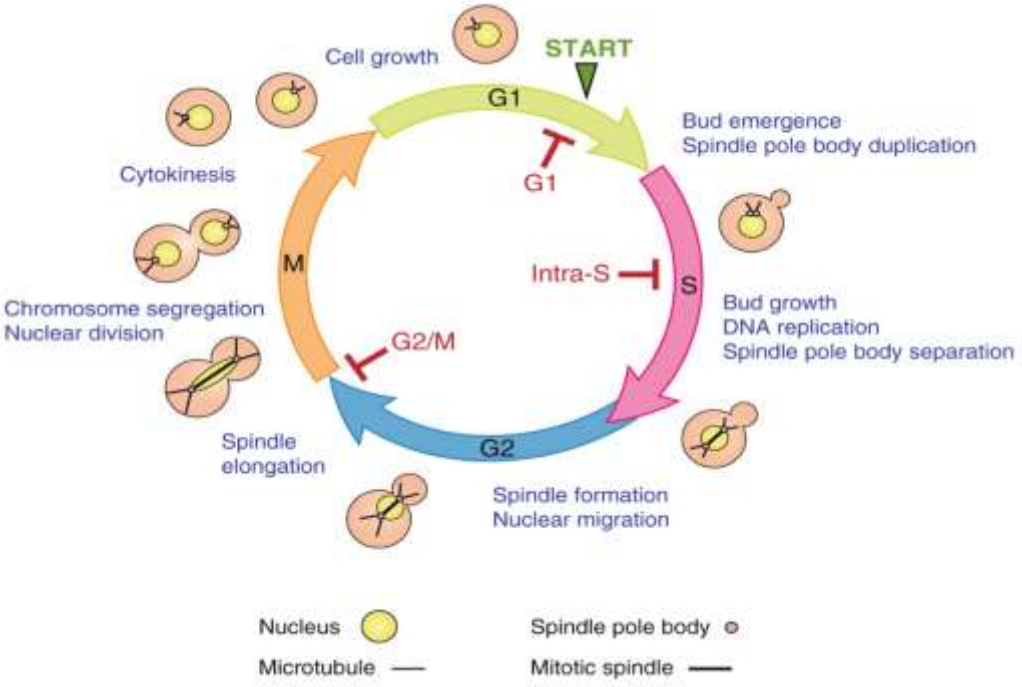

Figure 3. Schematic representation of the cell cycle and cell cycle checkpoints in *S. cerevisiae* (20).

The DDR results from the actions of many checkpoint and repair proteins which are evolutionary conserved from *S. cerevisiae* to vertebrates (4, 19). Thus, significant findings in yeast can be extrapolated to higher order systems. These proteins have various roles including as sensors, adaptors/mediators, and effector kinases. Sensing of the DNA damage results in a phosphorylation cascade that recruits many checkpoint proteins to the damage site and cell cycling machinery (Figure 4). The principal proteins in *S. cerevisiae* involved in the early steps of DSB checkpoint activation are listed in Table 1 along with their human homologues. The DNA damage response (DDR) pauses cell cycling to shift cellular priority to the rapid detection and repair of DNA damage in order to maintain genome integrity (4).

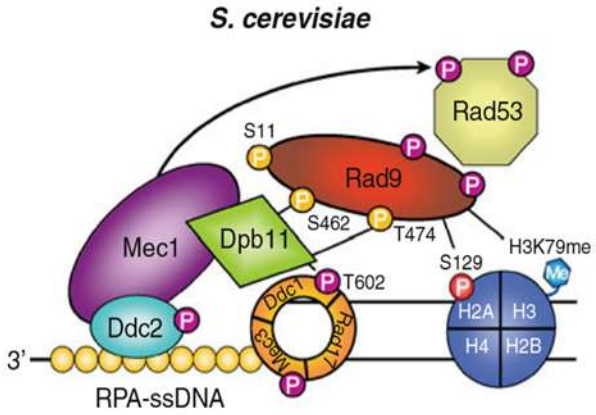

Figure 4. Schematic of cell cycle checkpoint proteins at a DNA damage site (20).

Table 1: Some of the relevant principal proteins in *S. cerevisiae* involved in the early steps of DSB checkpoint activation (20).

Class of protein	*S. cerevisiae*	Proposed function(s)	*H. sapiens*
Sensors	Mec1-Ddc2	Principal PIKK complex involved in sensing DNA damage and transducing the checkpoint signal. Mec1 binds Ddc2, which mediates its recruitment to sites of damage	ATR-ATRIP
Sensors	Rad24-Rfc2-5 (RFC-like complex)	Loading of Ddc1-Rad17-Mec3 (9-1-1) complex onto DNA. Role in DNA damage signaling.	RAD17-RFC2-5
Sensors	Ddc1-Rad17-Mec3 (PCNA-like complex)	Heterotrimeric complex, structurally related to PCNA, also called 9-1-1. DNA damage signal transduction and recruitment of other checkpoint proteins	RAD9-RAD1-HUS1
Adaptors/Mediators	Rad9	Molecular adaptor/mediator required for DNA damage signal transduction and DSB repair. Required for Rad53 and Chk1 activation.	53BP1; BRCA1; MDC1
Effector	Chk1	Effector kinase involved in signal transduction.	CHK1

Disease can be a result of deficient DNA repair systems

Many human genes related to disease have orthologs in *S. cerevisiae*, and high conservation of regulatory and metabolic systems in eukaryotes has contributed to widespread studies of these genes in lower, simpler systems. Several diseases have been identified that stem from deficient DSB repair (33). Human and yeast cells with defective DSB repair genes exhibit many similar phenotypes. Cells that lack genes involved in both pathways, such as *RAD50*, *MRE11*, or *XRS2* (*NBS1* in humans), can have devastating effects such as promoting the development of Nijmegen breakage syndrome (NBS) (33). In humans a defect in *SGS1* gene homologs, helicases involved in the HR pathway, can lead to Werner's or Bloom's Syndrome. Both diseases increase patient risk for certain types of cancer (21). In humans and mice, cells having a mutation that leads to a defect in NHEJ, such as *YKU70* or *YKU80*, have been shown to have an increase in cancer incidence as well as Severe Combined Immunodeficiency (SCID), a disease caused by an

inability to produce the normal assortment of antibodies (22). Certain cancers are associated with mutations in the BRCA1 and BRCA2 genes, which are responsible for assisting hRAD52 with its role in hRAD51 binding to ssDNA near DSB sites (39, 40). Mutant yeast cells defective in HR exhibit common characteristics such as slower growth and sensitivity to clastogenic chemicals. *RAD52*-deficient cells are categorized as extremely sensitive to X-rays and DNA damaging agents due to their loss in cell viability and increased rate of chromosome loss. *rad55, rad57* and *rad59* mutants are categorized as modestly sensitive to DNA damaging agents. A previous study has suggested that diploid *rad51* mutants may spend more time in G_2 phase, possibly because unrepaired DSBs in the cells are causing constitutive activation of the cell cycle DDR (45). Previous work in the L. K. Lewis lab also revealed that several *RAD52* group mutants have elevated levels of G_2 cells during growth in standard media under optimum conditions, without exposure to exogenous DNA damaging agents (6, 35, 36).

Yeast as a model system

There are several advantages to using yeast, *Saccharomyces cerevisiae,* as a simple eukaryotic model system. Yeast are commercially readily available and large quantities can be grown cheaply which is accommodating to a lab budget. Yeast cells are also non-pathogenic and can be handled with ease. The yeast genome contains a haploid set of 16 well-characterized chromosomes presenting a way to do sophisticated genetics assays in a eukaryotic system that is well-defined. Yeast are particularly well-suited for molecular genetics studies for a multitude of reasons. They have a rapid proliferation rate, which allows studies of phenotypic effects of mutations that affect senescence and future generation cell vitality to be performed with ease as compared to other eukaryotes.

The approximate doubling time of yeast during exponential phase, ~90 minutes in rich broth and ~140 minutes in defined synthetic media (glucose complete), allows these studies to be completed within a relatively quick time frame. Budding yeast cells also have the advantage of being morphologically different from other cells. Discerning cell phase (G_1, S, and G_2/M) is possible simply by visualizing the cells using a phase contrast microscope. In animal cells, G_1, S, and G_2 phases do not have an obvious effect on cell morphology and must be distinguished with staining techniques. Yeast cells have a high transformation efficiency ($>10^5$ transformation events possible per µg of DNA) as well as a natural tendency to perform integrative recombination with transformed DNA via homologous recombination. Plasmids or DNA fragments with foreign DNA sequences flanked by cloned yeast sequences can be inserted into specific locations in the chromosome at will. Stable crosses can be carried out with ease by mixing haploid *MATa* and *MAT*α strains with the genetic makeup of one's choosing and complementary auxotrophic mutations. Diploid colonies are selected for by the resultant prototrophic phenotype. This enables the relatively easy construction of a diploid genome with heterozygous or homozygous alleles at gene loci of choice. All of these traits make yeast particularly receptive to gene cloning and genetic engineering as evidenced by the fact that mammalian genes are routinely introduced into yeast cells for analyses of their functions. The two sexes, *MATa* and *MATalpha* cells, present an opportunity to confirm study results in two similar haploid systems. Yeast strains that have a particular genetic trait of interest can be stored indefinitely for future study by being transferred into and kept in 15% (v/v) glycerol in -60^o C temperature or lower. Yeast cells are later easily revived by transferring a small amount of frozen culture to a plate for growth (30).

Goals of this project

Major goals of this project were to quantitate changes in cell cycling and cell morphology in *S. cerevisiae* mutants that are deficient in DNA double-strand break repair, especially cells defective in HR, as well as cells that are deficient in both DNA repair and DNA damage checkpoint responses. In initial work, the observation that DNA repair-deficient *rad52* mutants spend more time in G_2 phase than wildtype cells was investigated. A high percentage of G_2 cells were observed in both haploid and diploid *rad52* mutants. In haploid cells, overall cell doubling times for *rad52* mutants during log phase growth were found to be 150% longer then in wildtype (WT) cells. Quantitation of the time spent in each phase revealed that *rad52* and WT cells spend similar amounts of time in G_1 and S phase, but *rad52* cells spend 2.7 times longer in G_2.

To test our hypothesis that the increase in G_2 cells is due to higher levels of unrepaired DSBs leading to constitutive activation of DNA damage checkpoints, mutations in seven known checkpoint genes were combined with *rad52* mutations to create *rad52 ddr* double mutants. G_2 cells were reduced to near WT levels in all seven *rad52* DNA damage checkpoint double mutants tested.

The possibility that inactivation of other members of the RAD52 group might also lead to high levels of G_2 cells was also examined. *rad51*, *rad54*, *rad55*, *rad57*, and *rad59* mutants also exhibited large numbers of G_2 cells and spent approximately 2 times as much time as WT cells in G_2 phase during log phase growth.

Cells' nuclei were stained with DAPI and analyzed microscopically to compare WT and *rad52* cells' nuclear morphologies. These experiments demonstrated that the

nuclear structures found in *rad52* cultures were consistent with the findings of past studies on Xray- and ultraviolet light-induced G_2 arrest of yeast cells. Furthermore, many log phase *rad52* cells appeared to be enlarged when cell sizes were measured using phase contrast microscopy. Interestingly, only about half of the G_2 phase *rad52* cells were enlarged. This result suggests that cells were pausing in G_2 but continuing to grow in size before eventually entering M phase and undergoing cell division. The results of this research can be translated into higher eukaryotes such as humans in order to better understand repair systems and responses, and possibly help prevent the myriad of complicated diseases that stem from DNA damage.

II. MATERIALS AND METHODS

Reagents

Ethylenediaminetetraacetic acid (EDTA) and sodium hydroxide (NaOH) were purchased from EMD Chemicals, Inc. (Darmstadt, Germany). Dimethyl sulfoxide (DMSO) and lithium acetate (LiAc) were obtained from Alfa Aesar (Heysham, Lancashire). Sodium dodecyl sulfate (SDS) was obtained from J.T. Baker (Center Valley, PA). Sodium acetate anhydrous, and glacial acetic acid were purchased from Mallinckrodt-Baker, Inc. (Paris, KY). The sonicated salmon sperm carrier DNA was obtained from Agilent Technologies (Santa Clara, CA). Ethidium bromide (EtBr) was obtained from IBI Scientific (Peosta, IA). Sodium chloride, sodium citrate dihydrate, Tris-HCl, and the Qubit dsDNA BR Assay Kit were purchased from ThermoFisher Scientific (Fair Lawn, NJ). Ammonium sulfate, isopropanol, formamide, and Trizma base were purchased from VWR International (West Chester, PA). Boric acid, maleic acid, polyethylene glycol (PEG 4000), Sarkosyl (N-lauryl-sarcosine), and Tween 20 were purchased from Sigma-Aldrich Chemical Co. (St. Louis, MO). Agarose LE was purchased from Gold Biotechnology (St. Louis, MO). TAE (50X) buffer was purchased from Omega (Cowpens, SC). Ethanol was obtained from Texas State University (San Marcos, TX). DIG High Prime DNA Labeling and Detection Starter Kit II, PCR DIG Labeling Mix, and DNA Molecular Weight Marker III were purchased from Roche Applied Science (Penzberg, Germany). RNase A was purchased from Sigma-Aldrich Chemical Co. (St. Louis, MO). Restriction enzymes, dNTPs, $MgCl_2$, Vent polymerase, Taq DNA polymerase, 6X loading dye, and 2 log DNA ladder were purchased from New England Biolabs (Beverly, MA). ExTaq DNA polymerase was obtained from Takara

(Madison, WI). All primers (Table 1) were created by Integrated DNA Technologies (IDT) (Coralville, IO). All amino acids, and ampicillin (Amp) were purchased from Sigma-Aldrich Chemical Co. (St. Louis, MO). D-(+)-glucose, soy peptone, and yeast nitrogen base were made by Amresco (Solon, OH). Bacto yeast extract was manufactured by Becton, Dickinson, and Company (Sparks, MD). Agar, molecular biology grade was obtained from Teknova (Hollister, CA). QIAprep Spin Miniprep Kits were purchased from Qiagen (Hilden, Germany). DAPI staining solution was purchased from GeneTex (Irvine, CA). Molecular Probes ProLong Gold antifade reagent was purchased from Life Technologies (Eugene, OR). Phosphate Buffered Saline 10X liquid concentrate was purchased from OmniPur (Gibbstown, NJ).

Equipment

Horizon 11-14 gel rigs were from LabRepCo (Horshan, PA). The Sorvall Lynx 6000 floor centrifuge, Savant DNA 120 SpeedVac Concentrator, Qubit 2.0 Fluorometer, replica-plating tool, and velvet squares were obtained from Thermo Fisher Scientific (Fair Lawn, NJ). The MXX-123 analytical balance was purchased from Denver Instruments (Bohemia, NY). Vortexes and all incubators were purchased from VWR Scientific Products (Radnor, PA). The model 5424 centrifuge was purchased from Eppendorf (Hamburg, Germany). The UV Stratalinker 2400 was purchased from Stratagene (La Jolla, CA). The T100 Thermal Cycler, Trans-Blot Turbo Blotting System, and ChemiDoc XRS+ instruments were obtained from Bio-Rad Laboratories (Hercules, CA). The RED imaging system was purchased from Alpha Innotech (San Jose, CA). HB-1000 Hybridizer was purchased from UVP Laboratory Products (Upland, CA). The E-

Class shaker, Orbit Environ Shaker, and Lab Rotator were made by Lab Line Instruments (Tripunithura, India). The orbital shaker and digital dry baths were purchased from BioExpress (Kaysville, UT). The microscope used for DAPI imaging was an EVOS FL digital LED-based transmission and fluorescence microscope purchased from Advanced Microscopy Group (Mill Creek, WA). The other microscope was a United Scope model M837T phase contrast microscope (Hopewell Junction, NY).

Yeast Strains, Plasmids and Primers

All DNA primers used in this study are listed in Table 1. PCR confirmation using primers RAD52E and LEU2A was done to verify the *rad52* deletion in BY4742 strains not containing the RAD52 plasmid. PCR confirmation was done with both RAD52E + LEU2A and RAD52U1 + LEU2A primer sets in the double mutants. BY4741 *rad52* knockouts were also double verified by PCR in this fashion. Primers used in this project are listed in Table 1. All single mutants and wild-type strains were available in the strain deletion libraries obtained from Open Biosystems (6).

All original library strains and new strains created for this project are listed in Table 2. All plasmids used in these experiments were isolated from *E. coli* cells by alkaline lysis (41) (Table 1). Most yeast strains used for the project were derivatives of BY4741 and BY4742 (57) (Table 2). Double mutant yeast strains were constructed by transforming seven different checkpoint single mutant strains from a deletion yeast strain library with a plasmid fragment containing the *RAD52*Δ*::LEU2* insertion derived from the plasmid pΔ52L (6). pΔ52L was cut with NotI and ApaI prior to transformation into cells. The seven checkpoint mutants included *rad9, rad17, rad24, mec3, ddc1, dun1* and

chk1 cells. Two versions of each *rad52*/*ddr* double mutant were made, one with a functioning *RAD52* gene expressed via the galactose promoter on a *URA3* plasmid (p316GalyR52) and one without. Checkpoint single mutant strain numbers are listed in Table 2. Cells were spread to either glucose minus leucine or galactose minus leucine minus uracil plates to select for cells with a *LEU2* insertion and also to select for the plasmid and express Rad52 via the galactose promoter if applicable. Plates were placed at 30^{o}C for colony growth. Colonies were patched to fresh glucose minus leucine or galactose minus leucine minus uracil plates for further purification.

Table 2. List of PCR primer sequences. A complete list of primers used.

	Primer Sequence
5-rad52	CAGGAAACAGCTATGACC
3-rad52	GTAAATATTAATACGACACATGGAGGAA
tRad52A	CGCCAGCAGTGAAATCACCACAGTTTGGATA
tRad52B	CTTAATGATCTATTGTTTTTCCGAGTTGCCAT
tRad52C	CTCTTGACACGCTCTAATACGTAGTCTTGTGG
tRad52D	GACATCTTCCAGAAAAATTCATCTCCAAGACGAGGA
tRad52E	GTCAGCGTCAGTGACATGATGTTGTAGGTTGTA
tRad52F	AGTCATTAGTAAAGTAATCGAGATCAAGCTGA
Rad52U1	ATCGTCAGTTCTTACCCTCAGCCTGTTTGGTGAT
Rad52U2	CCCAAGATCTTGTACTGATCTTAGGTACTGCACA
Leu2A	TCCAGCGCCTCATCTGGAAGTGGGACAC
Leu2B	TTTGTTGCCATCTGCGTCCTTGGCCTCT
M13 forward primer	TTACTCATCGCCAAAGAGTCTGCTCTTC
M13 reverse primer	AGCGCGCAATTAACCCTCACTAAAG

Table 3. Yeast strain list. A complete list of *S. cerevisiae* strains used for this project.

Strain	Genotype Source
YLKL568 = BY4742, *MATα his3Δ1 leu2Δ0 lys2Δ0 ura3Δ0*	
YLKL567 = BY4741, *MATa his3Δ1 leu2Δ0 met15Δ0 ura3Δ0*	Open Biosystems
YLKL890 = BY4742, *rad9Δ::G418^r*	Open Biosystems
YLKL935 = BY4742, *rad17Δ::G418^r*	Open Biosystems
YLKL942 = BY4742, *rad24Δ::G418^r*	Open Biosystems
YLKL898 = BY4742, *mec3Δ::G418^r*	Open Biosystems
YLKL944 = BY4742, *ddc1Δ::G418^r*	Open Biosystems
YLKL885 = BY4742, *dun1Δ::G418^r*	Open Biosystems
YLKL1563 = BY4742, *chk1Δ::G418^r*	Open Biosystems
YLKL861 = BY4742, *rad52Δ::G418^r*	Open Biosystems
YLKL687 = BY4742, *rad51Δ::LEU2*	Open Biosystems
YLKL688 = BY4742, *rad54Δ::LEU2*	Open Biosystems
YLKL862 = BY4742, *rad55Δ::G418r*	Open Biosystems
YLKL863 = BY4742, *rad57Δ::G418*^{r}	Open Biosystems
YLKL1190 = BY4742, *rad59Δ::G418^r*	Open Biosystems
YLKL864 = BY4742, *rdh54Δ::G418^r*	Open Biosystems
YLKL860 = BY4742, *rad51Δ::G418^r*	Open Biosystems
YLKL1189 = BY4741, *rdh54Δ::G418^r*	Open Biosystems
YLKL1579 = BY4741, *rad52Δ::G418^r*,	Open Biosystems
YLKL1581 = BY4741 *rad52Δ::LEU2*	Open Biosystems
YLKL1582 = BY4742 *rad9Δ::G418^r rad52Δ::LEU2* + p316GalyR52	Open Biosystems
YLKL1583 = BY4742 *rad17Δ::G418^r rad52Δ::LEU2* + p316GalyR52	Open Biosystems
YLKL1584 = BY4742 *rad24Δ::G418^r rad52Δ::LEU2* + p316GalyR52	Open Biosystems
YLKL1585 = BY4742 *chk1Δ::G418^r rad52Δ::LEU2* + p316GalyR52	Open Biosystems

VL6α = *MATα ura3-52 leu2-3,112, trp1-289 his7-2*	(53)
S1 = *MATα ura3-52 leu2-3,112 trp1-289 his7-2 ade5-1 lys2::lnsE-4A*	(54)
BGW1-7a = *MATa ura3-52 leu2-3,112 his4-519 ade1-100*	(55)
YLKL477 = YPH102 = *MATα ura3-52 leu2-Δ1 his3-Δ200 lys2-801(amber) ade2-101 (ochre)*	(56)

Table 4. Plasmid list. A complete list of plasmids used in this study.

Plasmid	Genotype Source
pΔ52L (*rad52*Δ::*LEU2* deletion plasmid)	Ed Perkins
p316GalyR52 (*GAL1p::RAD52 URA3 CEN/ARS*)	Lab Plasmid

Cell Culture Solutions and Media

Non-selective YPDA yeast plate growth media contained 1% bacto yeast extract, 2% soy peptone, 2% D-(+)-glucose, 2% agar, and 0.001% adenine. YPDA broth was prepared as YPDA media but without agar. Synthetic dropout media was used for plasmid selection. Dropout mix was composed of 0.17% yeast nitrogen base without amino acids, 0.5% ammonium sulfate, 2% D-(+)-glucose, 2% agar, and all essential amino acids and bases used for strain selection. I some cases, yeast synthetic growth media contained 2% galactose, instead of 2% glucose.

E. coli cells were grown for the isolation of plasmids using TB + ampicillin (amp) broth (1.2% bacto tryptone, 2.4% yeast extract, 0.5% glycerol, 10% 0.017 M KH_2PO_4 + 0.072 M K_2HPO_4, 100 µg/mL amp) or for sustained growth on LB + amp plates (1% bacto tryptone, 0.5% yeast extract, 0.5% NaCl, 100 µg/mL amp + 1.5% agar).

Gel Electrophoresis

Gel electrophoresis was performed in Horizon 11-14 gel rigs using 0.7 – 2% agarose gels in 1X TAE buffer (40 mM Tris, 20 mM acetic acid, 1 mM EDTA) at ~120 - 150 V or 0.5X TB buffer (45 mM Tris, 45 mM boric acid) at ~250 V. Ethidium bromide (0.5 µg/ml) was used to stain agarose gels and images were captured on the Alpha Innotech Red Imaging system.

Chromosomal DNA Purification – Mini preps for PCR verification of gene knockout

An optimized protocol was designed by the Lewis laboratory (52) as follows. Three mL of yeast cells were pelleted the supernatant was removed, and 300 µL of 6% SET solution (6% SDS, 10 mM EDTA, and 30 mM Tris pH 8.0) was added. This mixture was incubated at 65°C for 15 minutes and transferred to a water/ice bath for 5 minutes. 150 µL of cold potassium acetate solution (3.0 M potassium acetate and 2.0 M acetic acid) was added, then the tube was repeatedly inverted for 10 s. The mixture was centrifuged at 21000X g for 10 minutes to pellet protein and cell debris. The supernatant (containing the nucleic acid component) was combined with 500 µL isopropanol and mixed for 30 seconds before being spun at 21, 000X g for 2 minutes. The supernatant was

removed and the pellet was washed with 500 µL 70% ethanol, then incubated at room temperature for 1 minute before the ethanol was removed. The remaining ethanol was removed through the use of a speedvac for 10 – 15 minutes until dry. The pellet was suspended in 50 µL TE buffer (10 mM Tris pH 8.0 and 1 mM EDTA), and 1 µL of 2 mg/mL RNase A was added to degrade RNA contaminants. This mixture was incubated at room temperature for 10 minutes. The pellet was allowed to dissolve at 4°C then stored at -20°C.

Plasmid DNA Isolation

An improved alkaline lysis protocol for *E. coli* plasmid DNA minipreps method from the Lewis laboratory was used that is very similar to the alkaline lysis method described by Green and Sambrook (55). Bacterial colonies were grown in 2-5 mL of TB broth + Amp in a tall tube overnight in a 37°C shaker. One-and-a-half milliliters of the culture was added to a microfuge tube and quick spun at 21,000X g for 15-20 seconds and the supernatant was removed. The bacterial pellet was resuspended in 100 µL of Solution I (50 mM glucose, 25 mM Tris (pH 8.0), 10 mM EDTA (pH 8.0) by scraping the bottom of each tube against a wire test tube rack until the pellet was thoroughly dispersed. The mixture was kept on ice to reduce the amount of nicked open circular plasmid DNA (51). Two hundred µL of freshly prepared solution II (0.2 M NaOH + 1% SDS) kept at room temperature was added. Tubes were closed and inverted rapidly five times to mix, and stored on ice for 1 minute. One hundred and fifty µL of ice-cold Solution III (3 M KOAc) were added and the tubes were inverted rapidly several times to

mix. The samples were stored on ice for 3 minutes before centrifugation at 21,000X g for 10 minutes. The supernatant was transferred to a new tube except for the last 4-5 mm above the cell debris pellet. The DNA was precipitated by adding 400 µL of isopropanol, inverting several times to mix, and then spinning for 5 minutes at 21,000X g. The supernatant was removed using a 1000 µL pipettor, and the pellet was washed with 500 µL of 70% EtOH without disturbing the pellet. The sample was then centrifuged for 2 minutes at 21,000X g with pellets facing the same direction as in the first centrifugation so they were not dislodged. The supernatant was removed with a 1000 µL pipettor and put in the speedvac for ~10 minutes or until the pellet was dry. The pellet was resuspended in 50 µL of TE plus 2 µL of 2 mg/mL RNase A and vortexed. The pellet was incubated at room temperature for 10 minutes and then stored at -20°C.

PCR Amplification of *rad52Δ::LEU2* Insert for Verification of Gene Disruption

Reactions were done in 0.2 mL PCR tubes with 1 µM LEU2A and 1 µM Rad52U1 or rad52E primers, 1X Taq Polymerase Thermopol buffer, 0.25 mM dNTPs, Taq Polymerase (5 units), ddH_2O and 3 µL chromosomal DNA used as a template in a final volume of 50 µL. Five µL (10 µL for weak primer sets) of each sample were combined with 5 µL of ddH_2O and 2 µL 6X loading dye, mixed, and loaded onto a 0.8% agarose gel. Gels were stained with ethidium bromide for 15 minutes and imaged. PCR cycles were performed using 94°C for 30 seconds, annealing temperatures from 50°C – 56°C for 40 seconds, and an extension temperature of 72°C for 120-180 seconds (1 minute for the first kb with an additional 30 seconds added for each kb after). PCR was

conducted in an Applied Biosystems 2720 Thermal Cycler or a Bio-Rad T100 for 34 cycles.

Ethanol Precipitation to Clean Up Chromosomal DNA and DIG-labelled PCR Fragments

One twentieth volume of 3 M sodium acetate was added to samples (one tenth if suspended in ddH_2O as opposed to a buffer such as TE with salt). Two and a half volumes of cold 100% ethanol was then added to samples followed by vortexing. Samples were put on wet ice or kept at 4°C for greater than or equal to 15 minutes and then spun at 21,000 x G for 15 minutes. The supernatant was pulled and discarded. The pellet was rinsed with an appropriate volume (200-500 uL) 70% ethanol, spun for 3-5 minutes, and the supernatant again removed and discarded. Samples were then put in the speedvac for 5-10 minutes until visibly dry and resuspended in an appropriate volume of ddH_2O or TE.

Transformations of DNA into yeast cells

Yeast strains were transformed using a modified rapid lithium acetate/DMSO transformation method described by Tripp *et al*. (56). Cells were shaken overnight in 4 mL YPDA broth. One-and-a-half mL of the liquid culture was spun down and the growth media was removed. Cells were incubated in 0.2 M DTT at 42°C for 20 minutes. Cells were spun down and the supernatant was removed. Carrier DNA (50 µg) and transforming DNA (50-300 ng) were added to the pellet and the solution was mixed. A

master mix composed of 40% PEG 4000, 0.1 M LiAc, 1.0 mM EDTA, 0.1 M Tris (pH 7.5) was added to the pellet and DNA. A volume of DMSO was then added equivalent to 56 µL per transformation. This mixture was shaken for 15-30 minutes at 30°C, then at 42°C for 15 minutes. The mixture was spun down, the supernatant discarded, and 1 mL of YPDA broth was added. The samples were mixed and then incubated in a shaker for 30 minutes at 30°C. Cells were spun down and the broth removed. The pellet was resuspended in 200 µL ddH_2O and aliquots of the cells were plated to selective media at 30°C for colony formation.

Double imprint replica plating to find isolates with MMS sensitivity

At least 2 independent PCR-confirmed isolates from each *rad52* mutant were patched onto fresh synthetic dropout media plates and grown for 2 days at 30°C. The first plate with patches of cells grown on it would then be used as a master that was used to transfer the same pattern of cells onto to a sterile velvet. A second plate was placed on the velvet so cells could be transferred. A new velvet was obtained and the second plate was used as a master plate for cells to transfer to the new velvet. A third and fourth plate were placed on the new velvet and cells were transferred. The plates were put into an incubator at 30°C for 3 days to observe MMS sensitivity.

Streaking survival assay

Cells were streaked for single colonies in individual quadrants of plates and allowed to grow for 2-5 days at 30˚C and compared. Images were taken of the plates using a Canon Powershot G3 digital camera and saved as JPEG files.

Qubit Fluorometry for Quantification of DNA

Two assay tubes for the standards and one tube per sample that was tested were labeled. The Qubit working solution was prepared by diluting Qubit BR dsDNA reagent 1:200 in Qubit BR dsDNA buffer and vortexing. Two hundred µL of Working Solution was made for each standard and sample, plus an additional 200 µL. The standards were prepared by adding 190 µL of Working Solution to 10 µL of Standard #1 (0 ng/µL dsDNA) and 10 µL of Standard #2 (100 ng/µL dsDNA). Samples were prepared by adding 2 µL of DNA to 198 µL of Working Solution. One sample with a previously measured concentration was always included as well. Once standards and samples were prepared, all tubes were vortexed for 2-3 seconds and incubated at room temperature for 2 minutes. Tubes were inserted into the Qubit 2.0 Fluorometer and readings were taken.

Doubling time experiments

To determine the doubling time of a strain of yeast, 1 mL of YPDA broth was inoculated at $3x10^6$ cells/mL in 2 mL Eppendorf tubes and placed into a shaker in a 30◦C incubator. Each strain was tracked over a period of 8 hours starting at hour 3 using a hemocytometer and phase contrast microscopy. The following serial dilution scheme was used to make counting of cells easier and more timely. Starting at hour five, a 1:5 dilution was made by taking 60 uL aliquots from each isolate and mixing them with 240

uL ddH_2O before vortexing, sonicating, and loading onto the hemocytometer. At hours six and seven, 1:10 dilutions were made by diluting 30 uL cells into 270 uL ddH_2O. At hour eight, a 1:20 dilution was made by mixing 30 uL into 570 uL ddH_2O. Strains were immediately placed back into shaker after taking aliquots so as to not disturb doubling times. Four isolates from each strain were tracked so averages and standard deviations could be computed. Averages and standard deviations were then plotted on a semi-log scale in Microsoft Excel (y axis = the log of cells/mL $x10^6$, X axis = time in hours) and the best fit trendline plotted. Doubling times were obtained from the equation of the trendline.

DAPI Staining of Log Phase Yeast Cells to View Nuclear Morphologies

Innoculation of log phase cultures

Cultures were inoculated in a 2 mL tube containing 1 mL glucose complete broth at $3x10^6$ cells/ml. Cells were harvested in mid-log phase after 4 hours. Glucose complete broth was used because YPDA often produces substantial background during the staining process.

Formaldehyde Fixation prior to centrifugation to avoid displacement of nucleus

Cells were vortexed and sonicated at 22% amplitude for 10 seconds. One tenth volume of 36% formaldehyde per 1 mL yeast was added and tubes were left to sit 1-2 hours at room temperature. Cells were then washed twice with 1X Phosphate Buffered

Saline (PBS) before resuspending in original culture volume of PBS. Cells were spun at 10K x g for 3 minutes between washes. It is an option to leave cells at 4^{o}C at this point for use later in the day/week.

Before Staining

Cells were spun down and resuspended in an appropriate volume 70% EtOH, then incubated at room temp for 30-40 min. Following incubation, cells were spun down, the supernatant was removed, and they were resuspended in PBS. Cells could be stored at 4^{o}C at this point for use later in the day.

Staining

Cells were spun down at 10,000xg for 3 minutes, the supernatant was removed and 500 uL ddH_2O was added. Cells were then spun down again and the supernatant was removed. Two hundred microliters of 1X DAPI solution (Gene Tex Mix) was added to the pelleted cells and they were lightly vortexed to mix. Cells were then incubated 10 min at room temperature, spun down again and DAPI was pipetted out. Cells were washed with 1X PBS 2 times and ddH_2O once for 5 min each before spinning down to remove unbound DAPI. Cells were then resuspended in 3/10th of the original culture volume of ddH_2O.

Mounting

Prior to pipetting onto a slide, cells were lightly sonicated (using at least 300 uL volume in a 1.5 mL microfuge tube) (7 pulses at 20% duty cycle) and roughly 4 uL was pipetted at a time onto a slide. Then slides were passed rapidly through a bunsen burner flame a few times every five seconds until dry. Dilutions were made (1:5 and 1:10) and 4 uL aliquots were pipetted onto slides as well to be sure to obtain optimal imaging cell densities. Four microliters of ProlongGOLD antifade solution was pipetted on top of the dried sample before adding the cover slip. Cells must fix in the dark for 24 hours before imaging. The DAPI treated cells were exposed to as little light as possible, including when staining, before the 24 hour designated fixing period had passed. If the edges are sealed with a non-specific type of fingernail polish after fixation, slides will keep for several months.

III. RESULTS AND DISCUSSION

The primary focus of this project was to investigate the observation that mutant yeast cells defective in DNA double-strand break repair have a larger percentage of G_2 cells in liquid cultures than wild type cells. This indicates that the cells are spending longer amounts of time in G_2 phase. Previous work found that *rad52* and *rad51* cells, both defective in DSB repair, have a higher number of G_2 cells than wild type cells (43, 45-47). These mutants have the same phenotype that normal, healthy cells exhibit after being exposed to DNA damaging agents. We speculate that these DSB repair-deficient cells are pausing in G_2 phase due to the inability to repair endogenous DNA damage caused by reactive oxygen species (ROS) that are a normal byproduct of oxygen metabolism and also by other mechanisms. This damage could potentially lead to a constitutively activated DNA damage response. Major goals of this project were to quantitate the changes in cell cycling and cell morphology in *S. cerevisiae* mutants that are deficient in DNA double-strand repair, especially cells defective in HR, as well as cells that are deficient in both DNA repair and DNA damage checkpoint responses.

Initial experiments by undergraduate Paige Hall tested the percentage of large budded (G_2) cells in *rad52* cell cultures from different strain backgrounds isolated from around the world to test if this high percentage was conserved. Cells were inoculated into YPDA broth at $3x10^6$ cells/mL and shaken at 30^oC for 4 hours to get the cells into mid log phase. Cells were then examined using phase contrast microscopy. An example of the types of images analyzed for these experiments that were taken with the phase contrast microscope is shown in Figure 5.

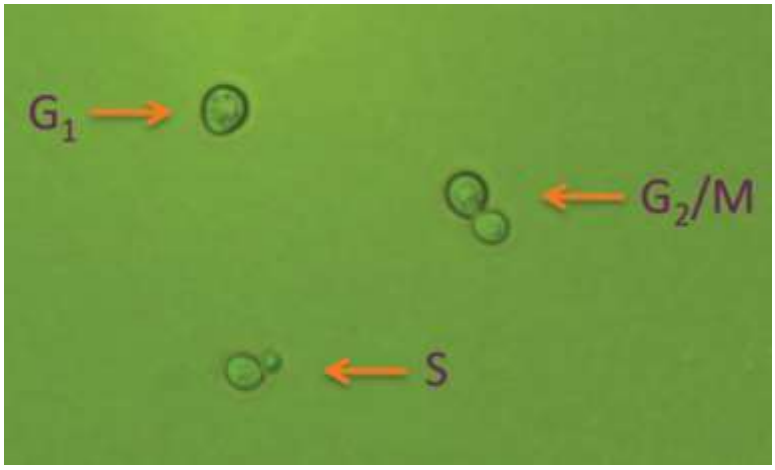

Figure 5. Example of different cell cycle phases as determined using phase contrast microscopy. Unbudded cells are classified as G_1, small-budded cells are in S phase and large-budded cells are in G_2 or M phase.

Cells were classified as being in G_1, S, or G_2/M based on their cellular morphologies. Cells in G_2 and M have large buds and are defined as cells in which the bud is $\geq$ 50% of the size of the mother cell (43). G_2 and M phase cells are grouped together due to the fact that they can only be distinguished by analyzing their nuclear morphologies, which cannot be done with standard phase contrast microscopy. M phase happens so rapidly that the vast majority of large-budded cells visualized are in G_2 phase (Figure 6). G_2 and M cells can be distinguished by applying nuclear stains that probe internal morphologies such as DAPI to visualize nuclear separation.

Figure 6. Timeline of the cell cycle phases G_1, S, G_2 and M. Length of line segments corresponds to the amount of time spent in each phase during log phase growth at 30°C. M happens very quickly with respect to the rest of the cell cycle.

The experiments showed that *rad52* mutants in each of the 5 backgrounds had about the same increase in percentage of G_2/M cells, many of them with a distended, or enlarged phenotype (Figure 7). WT cell cultures contained approximately 30% G_2/M cells, but each *rad52* mutant culture had ~ 50% G_2/M cells. This result indicated that the phenotype is conserved across different strain backgrounds.

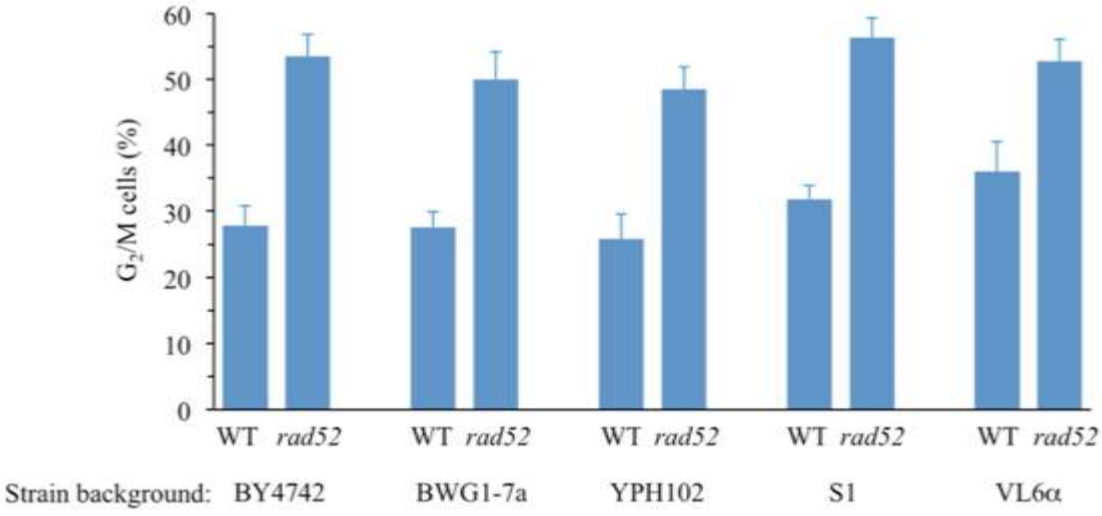

Figure 7. Yeast strain backgrounds BY4742, BWG1-7a, YPH102, S1, and VL6alpha were grown to log phase to investigate the phenomenon of an increase in the amount of G_2 cells found in cell cultures of DNA repair-deficient *rad52* mutants. The increased number of G_2/M cells was conserved across all strain backgrounds. Four cultures of each strain were analyzed. Averages and standard deviations are shown.

In addition to haploid yeast cells, diploid *rad52* $^{-/-}$ cells from two different strain backgrounds were also investigated. A high percentage of G_2 cells (~60%) was observed in each of the diploid *rad52* mutants as well.

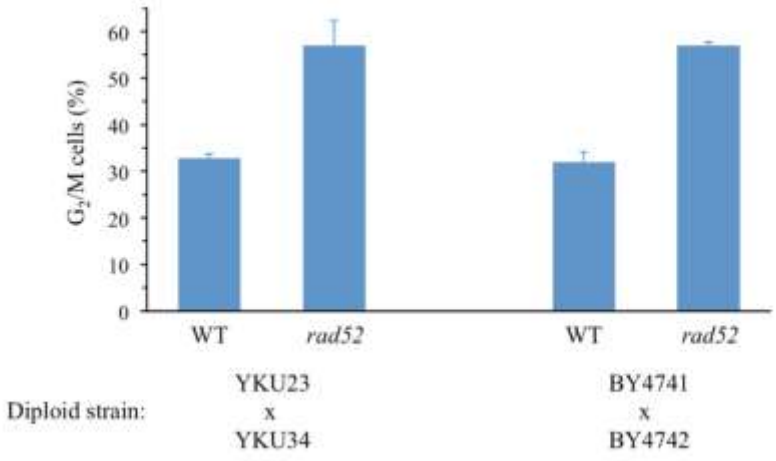

Figure 8. Diploid *rad52* $^{-/-}$ yeast strains exhibit high levels of G_2/M cells during log phase growth.

The first objective of this new project was to reproduce Paige Hall's findings. WT and *RAD52*-deficient BY4742 cells harvested from plates were counted and inoculated into YPDA broth at $3x10^6$ cells/mL, shaken for 4 hours at 30°C, and analyzed by phase contrast microscopy. It was observed that WT cell cultures had about 28% G_2/M cells while *rad52* cells had 50% G_2/M cells (Figure 9). This was consistent with the results that were previously observed.

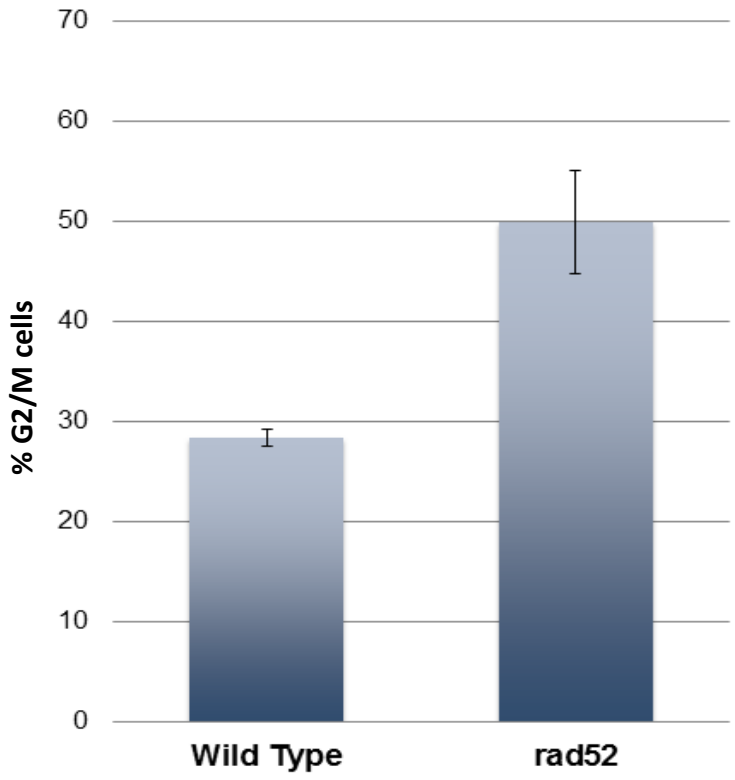

Figure 9. WT and *rad52* cultures were grown to mid-logarithmic phase and % G_2/M phase cells quantified. Four replicates of each strain were tested. Error bars indicate standard deviations.

Cell cycle doubling times during logarithmic phase growth were then calculated for WT and *rad52* cells. Cells were inoculated at $3x10^6$ cells/mL into YPDA broth and

cell titer was tracked using a hemocytometer over a period of eight hours, starting at hour three, when cells are growing exponentially. The time was then plotted against a logarithmic scale of cell titer. The equation of the best fit trendline was then used to compute the doubling time for each haploid strain (Figure 10). To calculate the doubling time, a value was plugged in to the Y variable of the equation and the resultant X value recorded. The first Y value was then doubled and plugged into the equation and the second X value recorded. The doubling time is the difference between X_2 and X_1. *rad52* mutants had 50% longer doubling times than WT cells (128 minutes to complete each cell cycle versus 83 minutes for WT cells).

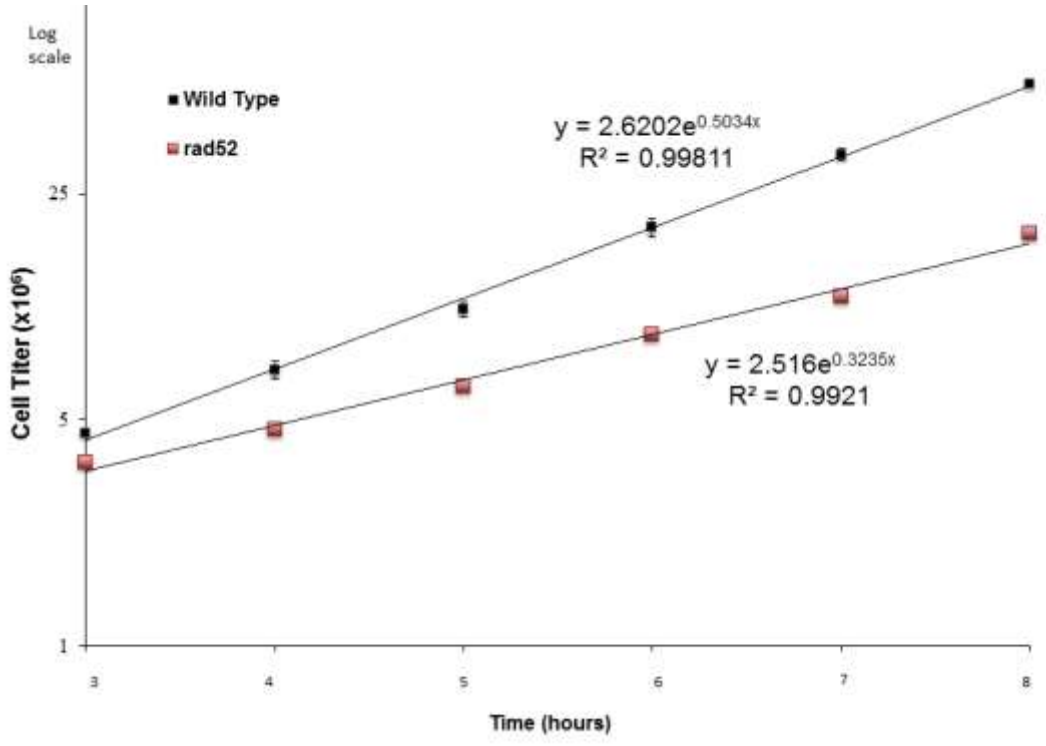

Figure 10. Plot of cell titer versus time for BY4742 WT and *rad52* cells. Four cultures of each strain were analyzed and results were averaged. Wild type cells had a doubling time of 83 minutes and *rad52* mutant cell cycles required 128 minutes.

The observation that DNA repair-deficient *rad52* mutants spend more time in G_2 phase than WT cells was then investigated in more detail. The percentage of cells in each cell cycle phase during growth in cell culture is proportional to the amount of time spent in that phase. Total cell cycling time (doubling time) and the percentages of cells in G_1 (unbudded), S (small-budded), and G_2 /M (large-budded) during logarithmic phase growth were used to calculate the minutes spent in each phase (Figure 11). M phase is very short so it was assumed most large-budded cells were in G_2. *rad52* cells spend 2.7 fold more time in G_2 phase than WT cells (63.8 minutes as compared to 23.5 minutes). By contrast, minutes spent in G_1 and S were similar in the two strains.

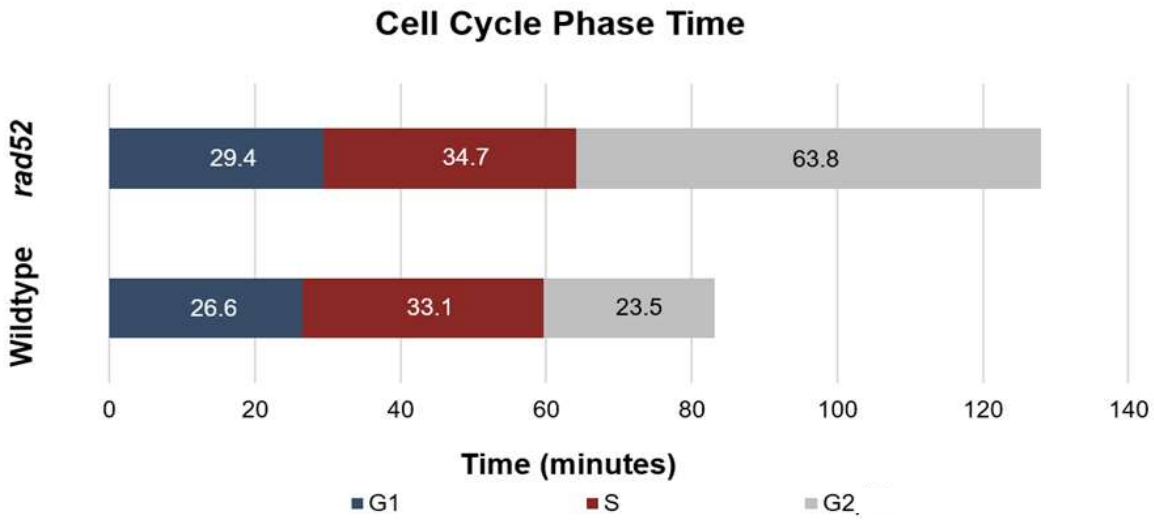

Figure 11. Time spent in each cell cycle phase for WT and *rad52* cells. *rad52* mutants spend approximately the same amount of time in G_1 and S phase as WT cells, but they spend about 2.7 fold more time in G_2 phase.

We wanted to investigate how the percentage of G_2/M cells changes as cells transition from stationary phase, through logarithmic phase, and back to stationary phase growth. WT and *rad52* cells were innoculated at $3x10^6$ cells/mL into YPDA broth and shaken for 48 hours. Aliquots were removed at 0, 4, 8, 12, 24, and 48 hours. Both percent G_2/M cells and cell titer (cells per mL) were calculated from aliquots (Figure 12). The percentage of large-budded cells continued to increase in *rad52* cells until hour 8, when they reached 67%. WT cells reached a peak percentage of 34% at hour 4.

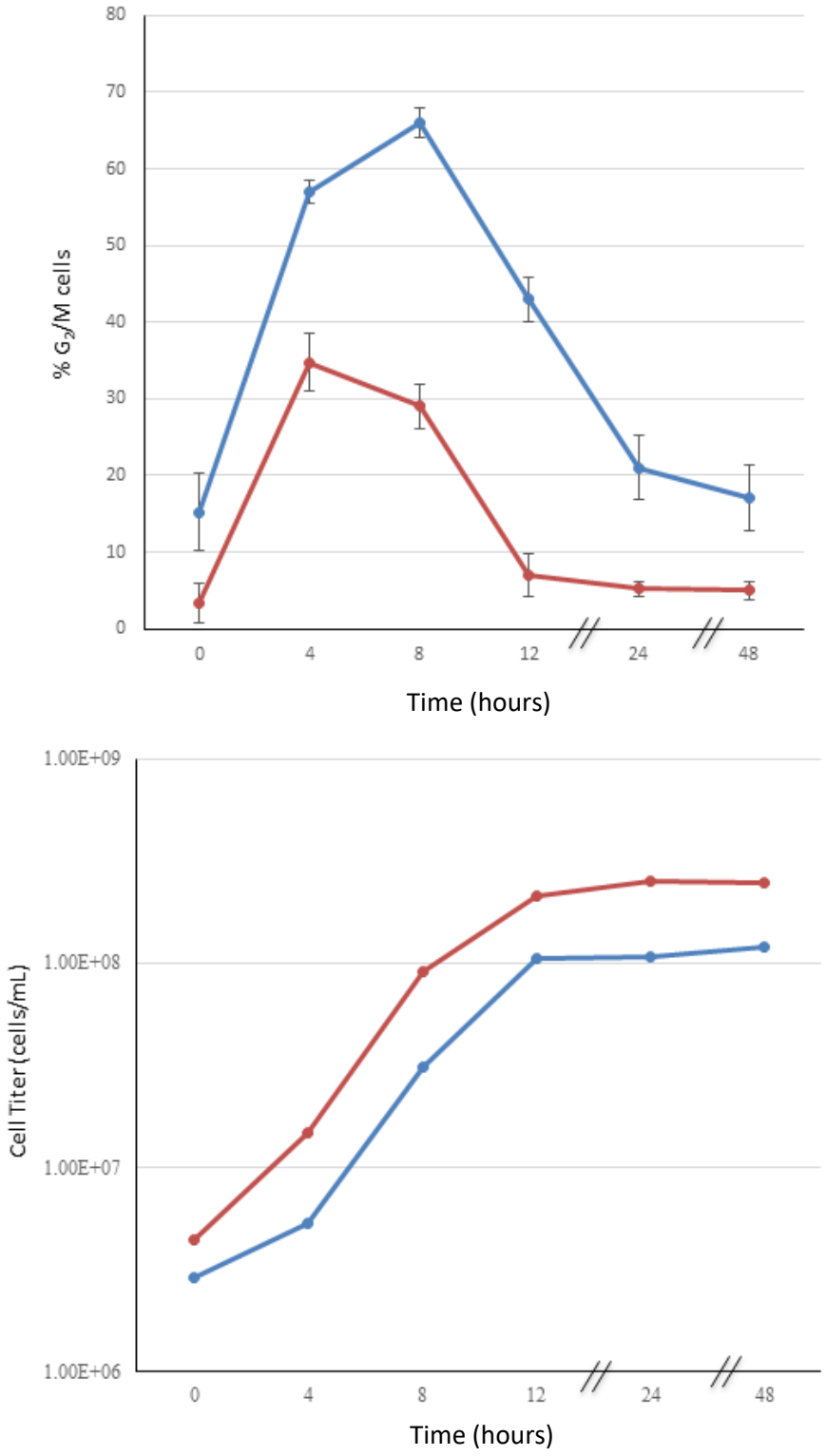

Figure 12. The percentage of G_2/M cells (top) and cell titer (bottom) were tracked for a period of 48 hours for 4 isolates of WT and *rad52* cells.

Rad52 protein works with several other proteins to repair DSBs via the homologous recombination pathway. Many of these proteins are members of the RAD52 group, which includes Rad50, Rad51, Rad52, Rad54, Rad55, Rad57, Rad59, Mre11, Xrs2, Rdh54 and the Rpa complex. The possibility that inactivation of other members of the RAD52 epistasis group might also lead to high levels of G_2/M cells was also examined. RAD52 epistasis group members that were tested are listed in Table 5 below with their corresponding protein function.

Table 5. RAD52 group members analyzed in the current study.

Rad52 Epistasis Group Member	Function
Rad52	catalyzes assembly of Rad51 onto DNA
Rad51	binds ssDNA; performs homology search
Rad54	strand invasion
Rad55	stabilizes Rad51 and ssDNA
Rad57	stabilizes Rad51 and ssDNA
Rad59	removes non-homologous ends from ssDNA
Rdh54	unwinds DNA to promote strand opening

Strains were inoculated into YPDA broth at $3x10^6$ cells/mL and grown to log phase before quantifying the percentage of G_2/M cells using a hemocytometer. *rad51, rad54, rad55, rad57*, and *rad59* mutants also exhibited higher percentages of G_2/M cells

than WT cells, with non-overlapping standard deviation error bars (Figure 13). *rdh54* mutants were the only cells that did not exhibit a strong increase. Rdh54 plays a role in homologous recombination in diploid cells and during meiosis (44). Haploid cells were tested in this experiment and *rdh54* haploids may not exhibit a phenotype for that reason. This hypothesis was addressed in further experiments described later.

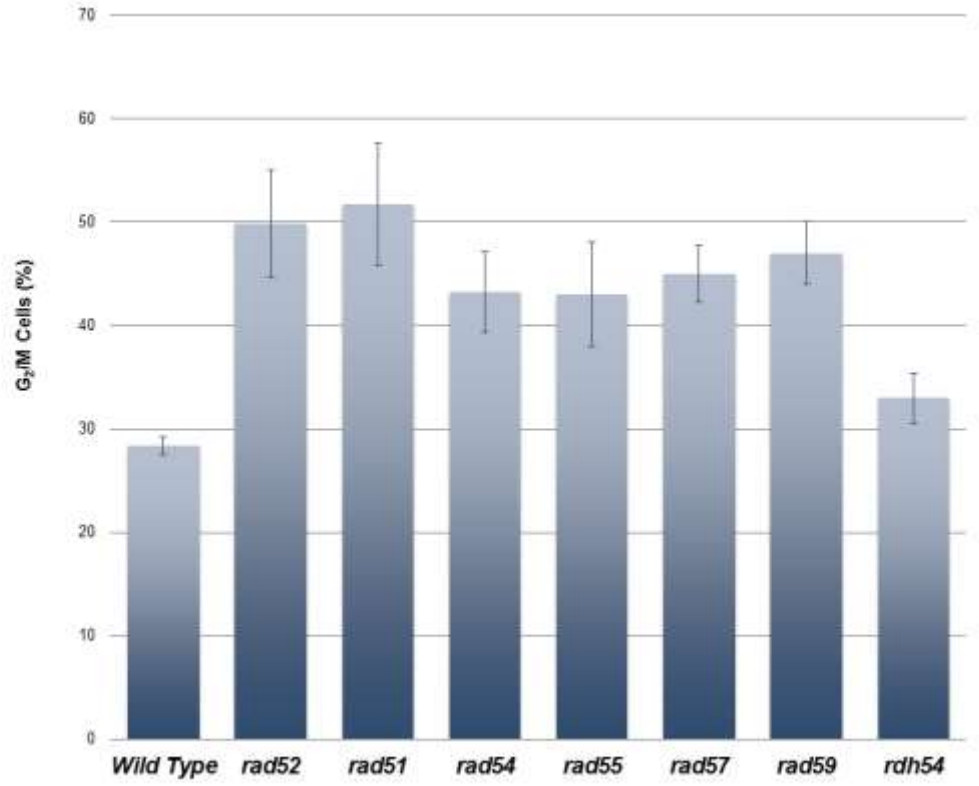

Figure 13. Quantification of G_2/M cells in recombination-defective RAD52 epistasis group mutant cell cultures. All strains had strongly elevated levels of G_2/M cells except *rdh54*. Four replicates of each strain were tested and averages and standard deviations are shown.

The next experiment measured how long each RAD52 epistasis group mutant was spending in G_1, S, and G_2 phase. To do so, doubling times were determined by inoculating each strain into YPDA broth at $3x10^6$ cells/mL followed by shaking at 30ºC. Cell titer was tracked using a hemocytometer and phase contrast microscopy for a period of 8 hours starting at hour 3 as before. The log of the cell titer was then plotted against growth time and the data fit to an exponential curve. The resulting equation of the best fit trendline was used to find the doubling time (Figure 14).

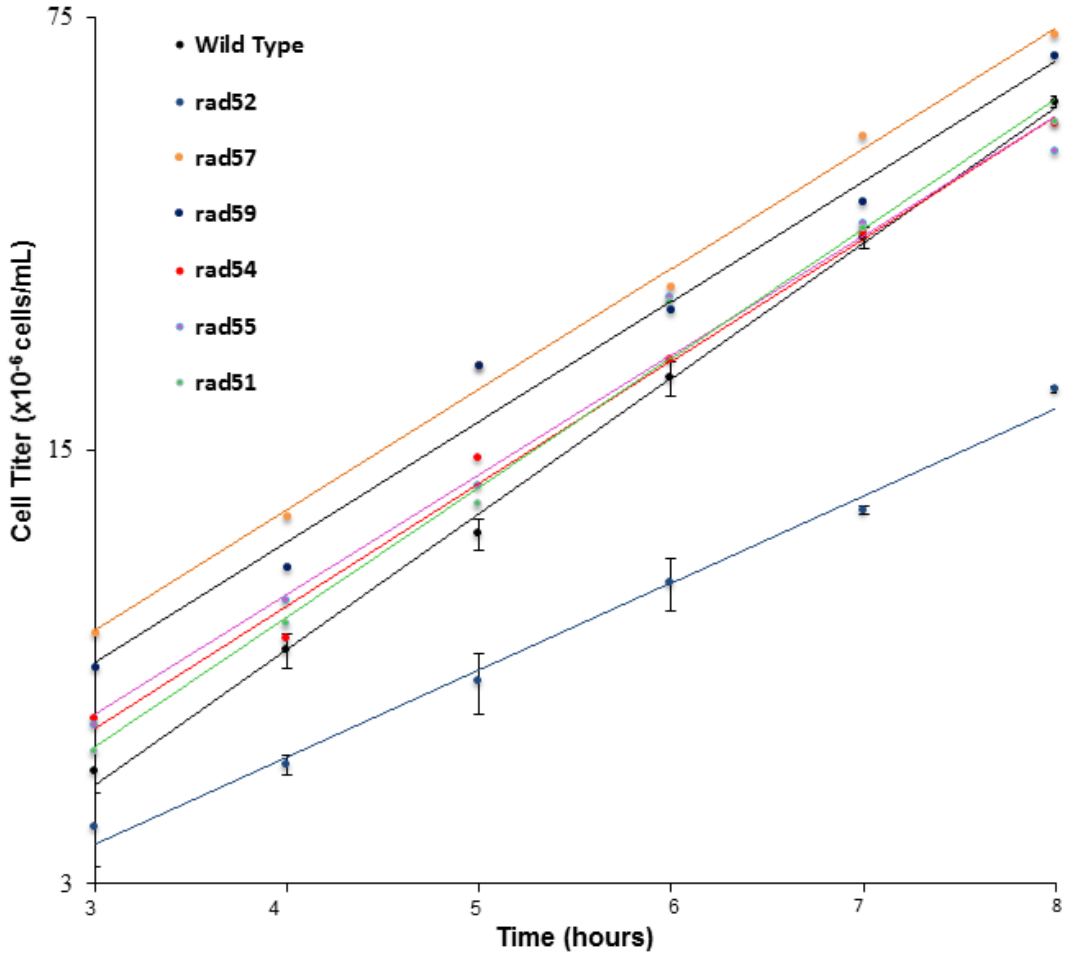

Figure 14. Graph of the log of cell titer tracked with a hemocytometer vs time. The equations of the best fit trendlines were used to find the doubling times of the RAD52 epistasis group mutants.

All of the RAD52 epistasis group mutants displayed elevated doubling times (~90 minutes as compared to ~83 min for WT cells). *rad52* cells differed from the others and exhibited a more extreme phenotype, with a doubling time of 128 minutes. Results are as listed in Table 6 below.

Table 6. Doubling times of RAD52 epistasis group mutants.

Rad52 Epistasis Group Member	Doubling Time (minutes)
WT	83
rad52	128
rad51	88.9
rad54	93.6
rad55	91.2
rad57	92.1
rad59	93.1
rdh54	90

Next, using the doubling times and cell cycle percentages, the length of time RAD52 epistasis group members were spending in each phase of the cell cycle was calculated, as done previously for *rad52* cells. While WT cells spent 24 minutes in G_2 phase, *rad51*, *rad54*, *rad55*, *rad57*, and *rad59* cells spent nearly twice as long in G_2 (ranging from 39.2 to 46.0 minutes).

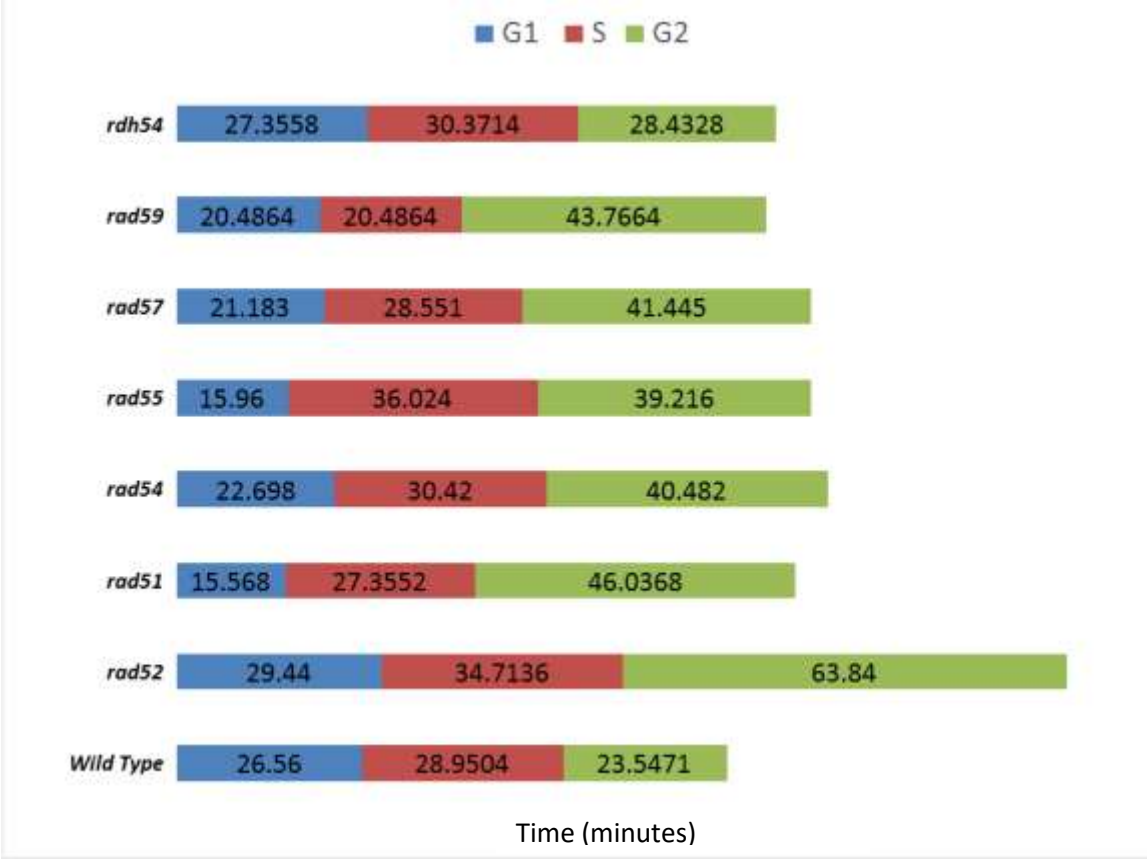

Figure 15. Time spent in each phase of the cell cycle by several RAD52 epistasis group mutants.

Most of the experiments discussed in this work thus far have involved the use of haploid BY4742 *MATα* strains. Haploid yeast cells are classified into two mating types called *MATa* and *MATα*. Experiments with the *MATα* mutants showed that *rad52* mutant phenotypes were much more extreme than in the other DSB repair mutants (*e.g.*, 128 minute doubling time versus ~90 min for other mutants). New experiments were performed to see if this extreme phenotype that *rad52* mutants exhibit would also be observed in BY4741 *MATa rad52* mutants. A new homemade *rad52*Δ*::LEU2* BY4741

MATa strain was created by transformation of WT cells with a fragment of the plasmid pΔ52LEU2. *RAD52* was inactivated by exploiting the fact that yeast cells undergo high rates of homologous recombination via inserting a functioning *LEU2* gene into the *RAD52* gene. A schematic of the approach used is shown below (Figure 16). The plasmid was cut with NotI and ApaI endonucleases and the resulting fragment was transformed into BY4741 cells using the LiAc and heat shock method as listed in chapter II. The flanking *rad52* regions surrounding *LEU2* underwent genetic exchange with the *RAD52* gene on chromosome XIII. This deletes a portion of the *RAD52* gene and inserts *LEU2* (Figure 16).

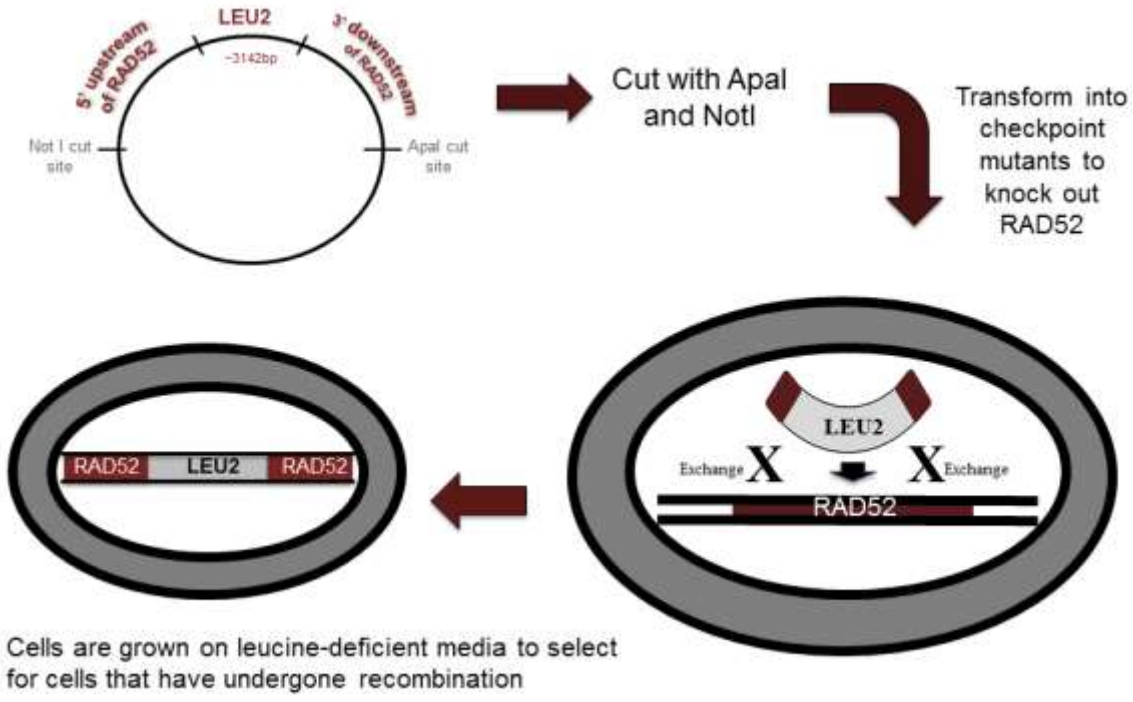

Figure 16. *RAD52* inactivation via transformation with a fragment of the plasmid pΔ52LEU2.

After transformation, cells were grown on leucine-deficient synthetic media to select for cells that underwent an exchange event and were successfully expressing the *LEU2* gene. Colonies that grew on leucine-deficient media were then streak-purified and confirmed to have the *RAD52* gene knocked out via polymerase chain reaction (PCR) using the chromosomal DNAs as templates. One primer for the PCR reaction corresponded to the *RAD52* gene (RAD52E) and the other to *LEU2* (LEU2A). There should only be a PCR product if the *LEU2* gene was inserted into the *RAD52* locus (illustrated in Figure 17).

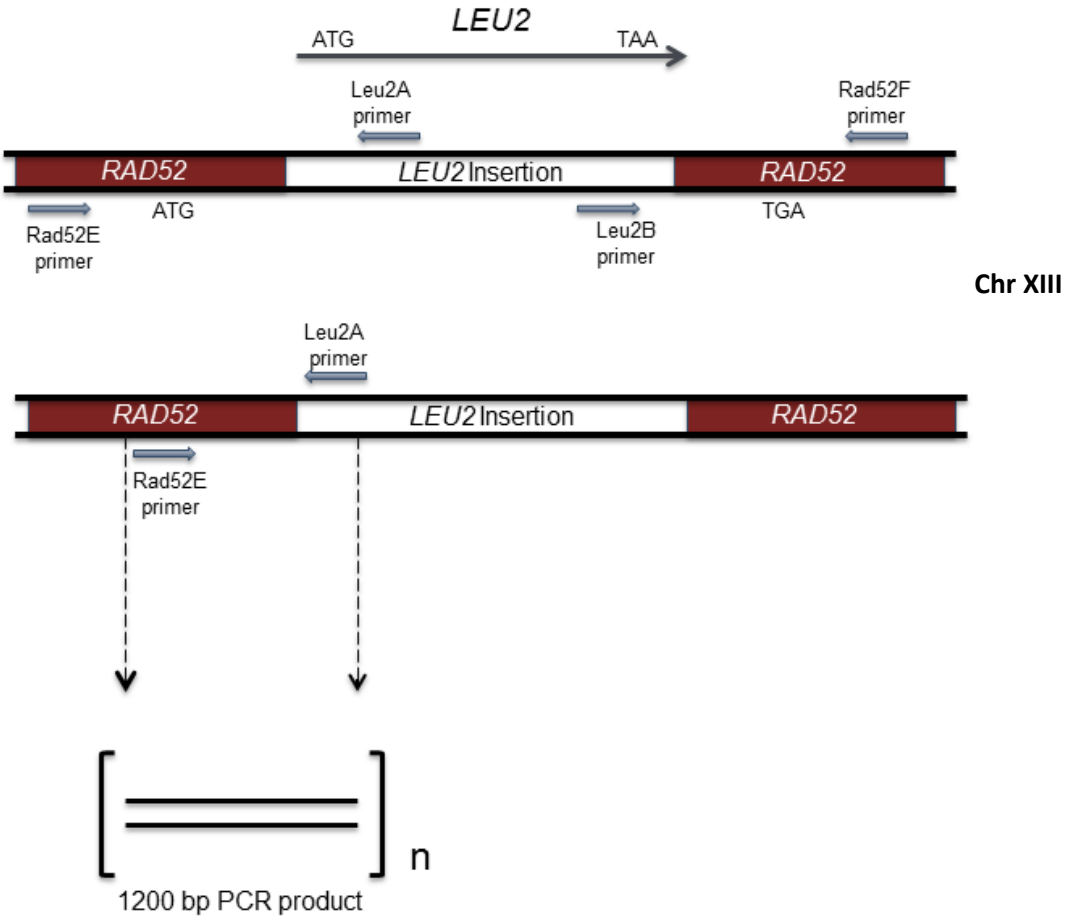

Figure 17. Logic behind verification of *RAD52* gene knockout via PCR. The selection of primers ensured that the 1200 bp product is only seen if the *LEU2* gene is inserted into the *RAD52* locus.

Several isolates exhibited a band at 1200 bp, which therefore confirmed that they had the *LEU2* gene inserted into the *RAD52* locus, inactivating the *RAD52* gene and thus making cells homologous recombination-deficient. Four confirmed isolates (5, 6, 7, and 8) were streak-purified and inoculated into YPDA broth at $3x10^6$ cells/mL and grown at 30°C for 4 hours to reach mid log phase as before to assess levels of G_2/M cells in each

culture. *MATa* WT, *rad51*, and a *rad52* mutant from a *MATa* yeast deletion strain library were also analyzed. Both *rad52* strains, as well as the *rad51* strain, exhibited higher levels of large-budded cells. The range of G_2/M percentages was similar to that seen in the earlier *MATα* strain experiments (45-55%). Results are depicted in the graph below (Figure 18).

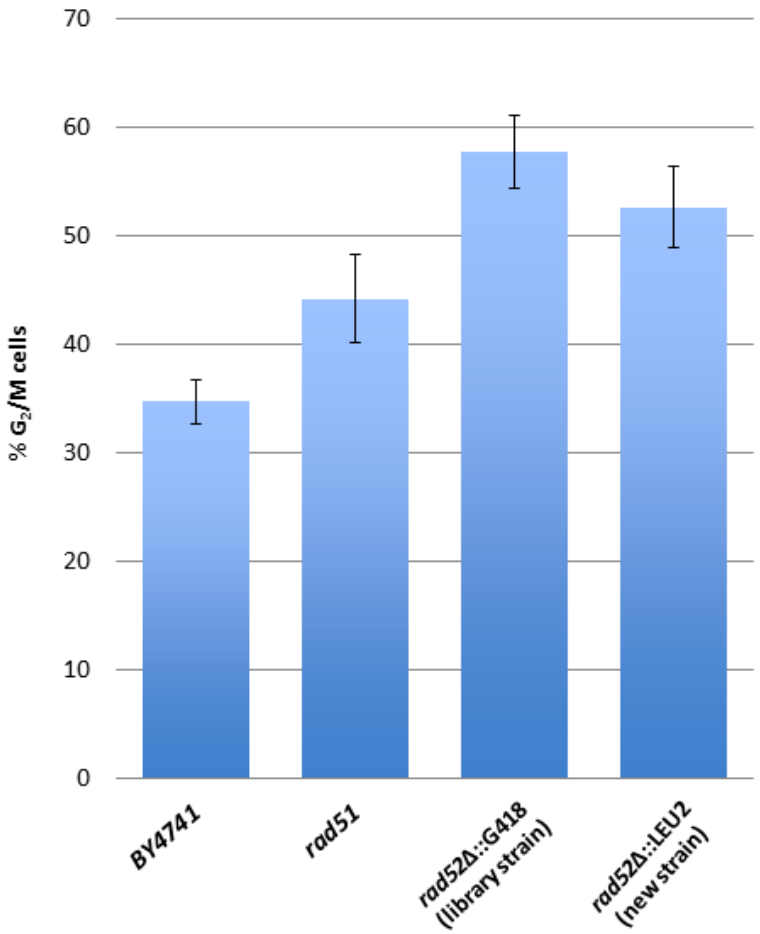

Figure 18. Percentage of G_2/M cells in BY4741 (*MATa*) WT, *rad51*, and two different *rad52* strain cell cultures. Four replicates were tested. Error bars indicate standard deviations.

The doubling times of the BY4741 (*MATa)* strains were determined to see how they compared to the doubling times in the BY4742 (*MATα*) strain background. Cells were inoculated at $3x10^6$ cells/mL into YPDA broth and shaken at 30°C as before. The log of the cell titer was plotted against time as shown in Figure 19. The equation of the best fit trend line was used to determine the doubling time of each strain. As seen previously in BY4742 cells, the BY4741 *rad52* mutants had a more extreme phenotype than *rad51* cells, with a doubling time of 115 minutes versus 85 minutes.

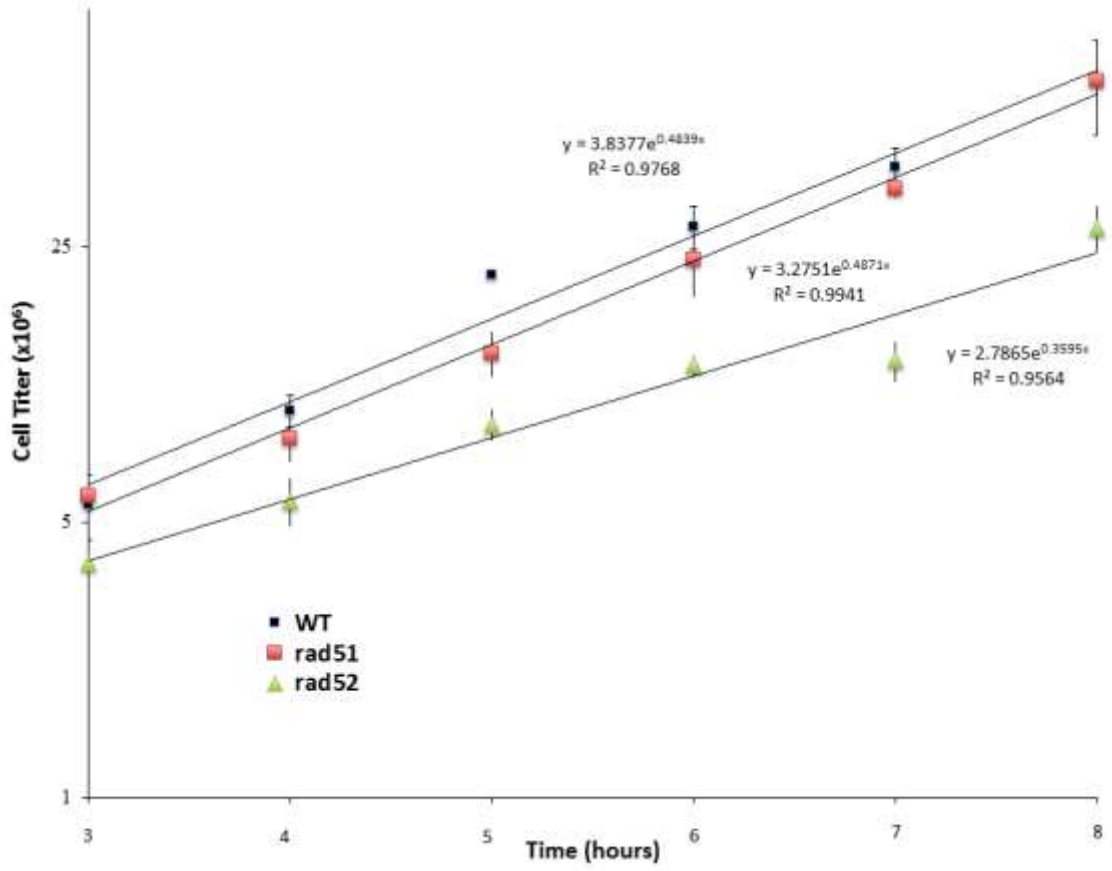

Figure 19. Growth curves used to calculate doubling times of BY4741 (*MATa*) strains. Cell cycle doubling times were calculated to be 85, 85, and 115 minutes for WT, *rad51*, and *rad52* cells, respectively.

Doubling times were multiplied by the percentage of G_2 cells present during logarithmic phase growth to obtain an estimate of the average time cells were spending in G_2 phase (Figure 20).

BY4741 *rad52* cells spent ~2.5 times the amount of time that WT cells spend in G_2. This is comparable to the ~2.7 times the amount of time BY4742 *rad52* cells spend in G_2 phase as compared to WT. G_2 phase in the *rad51* cells was also increased, but much less so than in *rad52* mutants. These experiments demonstrate that DSB repair-deficient *rad51* mutants exhibit high G_2 cells in both *MATa* and *MATα* strains. They also confirm that *rad52* cell phenotypes are more extreme than those seen in *rad51* cells in both cell types.

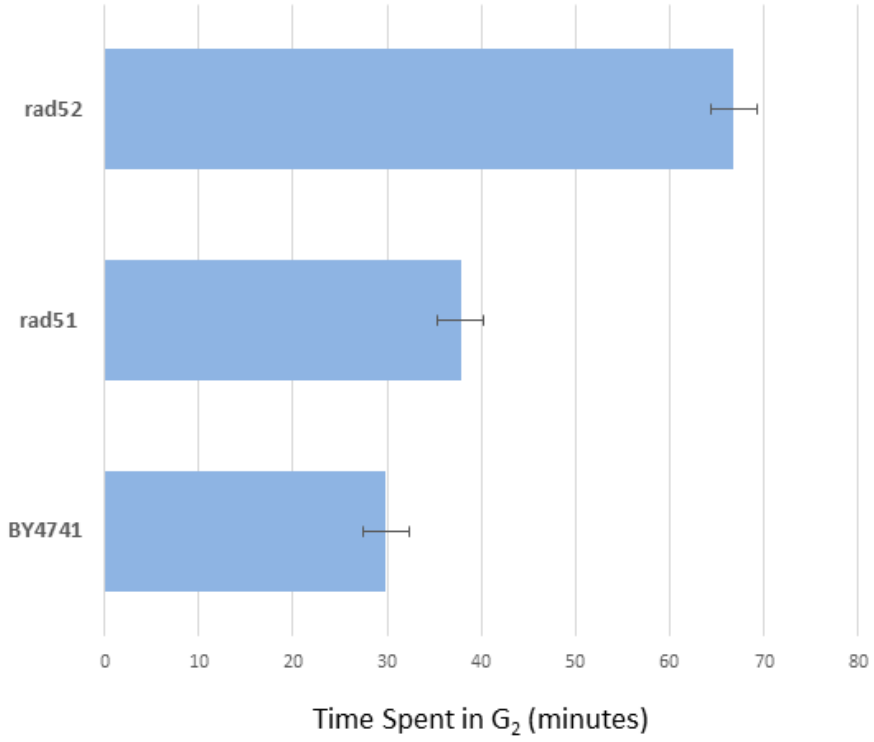

Figure 20. Time spent in G_2 phase for BY4741, *rad51*, and *rad52* cells. *rad52* cells spend ~2.5 x more time in G_2 than WT cells.

rdh54 cells were the only RAD52 group members whose time in G_2 was not statistically different than WT. However this gene is known to affect recombination in diploids, not haploids. We created WT and *rdh54/rdh54* diploids by mating *MATa* and *MATα* strains according to the mating protocol seen below (Figure 21).

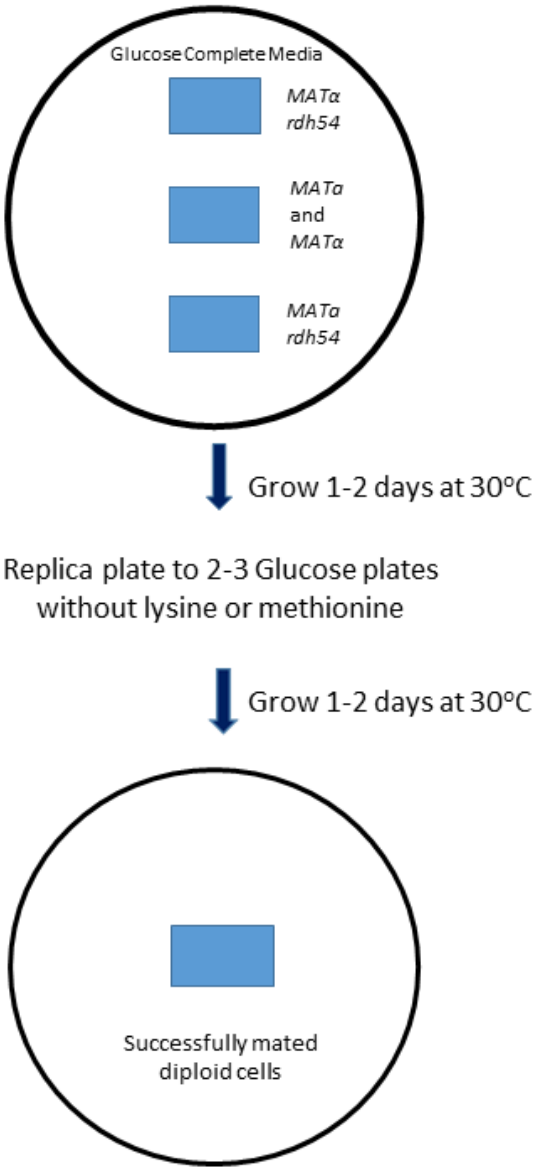

Figure 21. Schematic of mating protocol used for crossing BY4741 (*rdh54*) and BY4742 (*rdh54*) cells to obtain *rdh54* $^{-/-}$ diploid strains. BY4741 cells are *ura3 leu2 his3 met15* and BY4742 cells are *ura3 leu2 his3 lys2*. The *MATa* and *MATα* cells were mixed together in the middle rectangle of the glucose complete plate, grown for 2 days at 30°C to allow mating to occur, and were then replicated to a plate lacking lysine and methionine to select for diploid cells (*met15*$^{+/-}$ *lys2*$^{+/-}$ *ura3*$^{-/-}$ *leu2*$^{-/-}$ *his3*$^{-/-}$).

After streak purification of successfully mated colonies, levels of G_2/M cells during mid log phase were quantified. Diploid WT cells did not have a statistically different level of G_2/M cells as compared to *rdh54* $^{-/-}$ cells, with each strain displaying ~30% G_2/M cells (Figure 22).

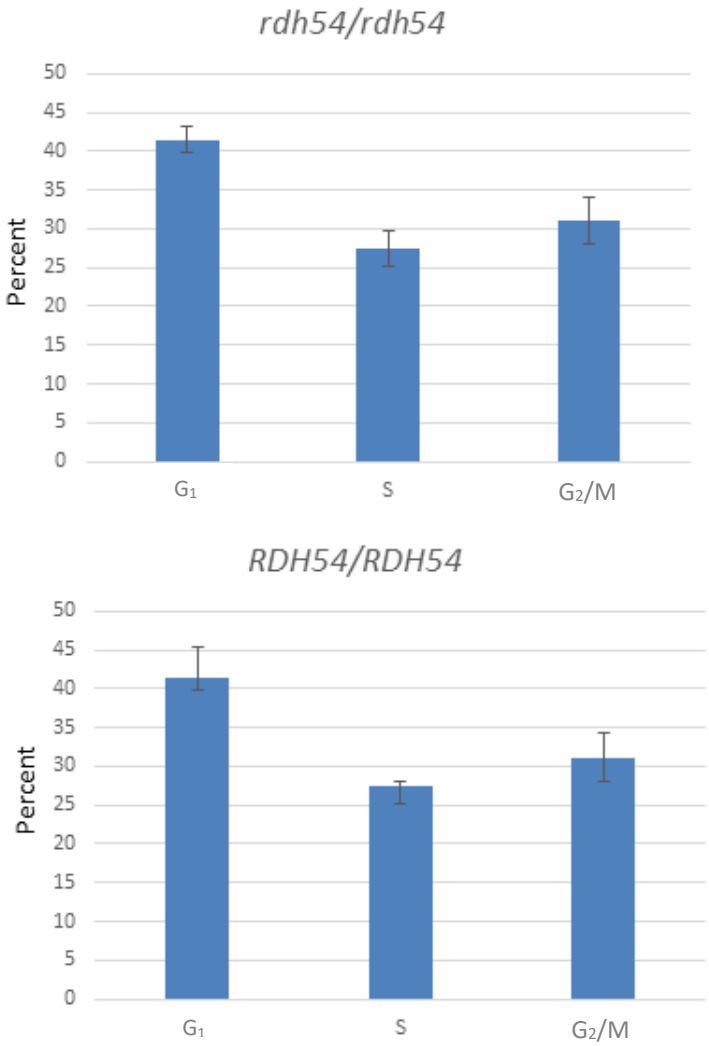

Figure 22. Levels of unbudded (G_1), small-budded (S), and large-budded (G_2) diploid WT and *rdh54*$^{-/-}$ cells during mid-logarithmic phase growth. *rdh54*$^{-/-}$ mutants exhibited WT levels of G_2/M cells.

These experiments have indicated that *rad52* cells and cells with other genes of the RAD52 epistasis group inactivated are spending extended amounts of time in G_2 phase, but the mechanism involved has not been examined. We hypothesized that unrepaired DNA DSBs in homologous recombination-deficient *rad52* cells may be causing activation of the DNA damage response (DDR) system, which causes cells to pause in G_2 phase in an attempt to repair the damage before moving on to M (mitosis) phase. The thought follows the fact that *rad52* cells grown under normal conditions are exhibiting a phenotype that wildtype cells exhibit after being exposed to DNA damaging agents such as X-rays or UV radiation. When log phase cultures of yeast (a mixture of G_1, S, and G_2/M cells) are exposed to radiation, many of the cells pause in G_2, causing G_2 cells to accumulate to higher levels in the culture temporarily (Figure 23).

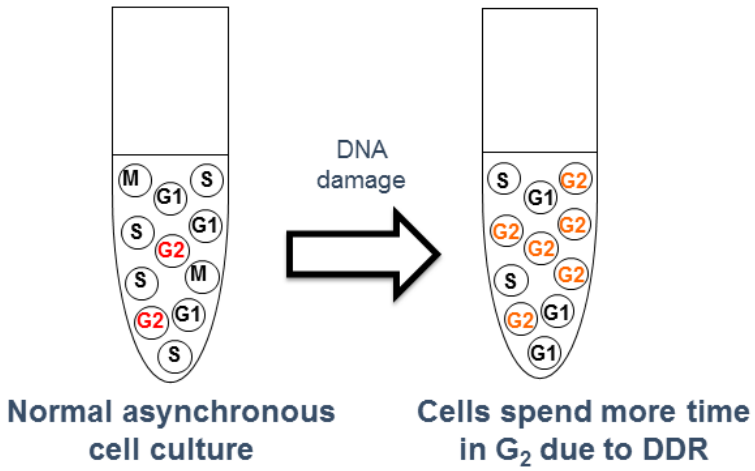

Figure 23. When exposed to DNA damaging agents, WT cells pause in G_2 phase due to a DNA damage response (DDR). This causes an increase in the number of G_2 cells found in culture. This phenomenon is similar to that exhibited by *rad52* cells in log phase growth, even though these cells have not been exposed to an exogenous DNA damaging agent.

To test our hypothesis that *rad52* mutants have high levels of G_2/M cells due to unrepaired DNA damage and thus a constitutively activated cell cycle checkpoint response, new double mutants were created. The *RAD52* gene was inactivated by insertion of *LEU2* in seven different *MATα* library strains that had DNA damage response genes knocked out. The strains in which *RAD52* was inactivated are listed in Table 4 with their corresponding gene functions. The strains created by this procedure were *rad52 rad9*, *rad52 rad17*, *rad52 rad24*, *rad52 mec3*, *rad52 ddc1*, *rad52 dun1* and *rad52 chk1* double mutants.

Table 7. DDR mutant strains in which *RAD52* was inactivated with their corresponding gene functions.

Deletion Strain	Protein Function
rad9	adaptor/mediator (required for chk1 activation)
rad17	sensor (part of 911 complex)
rad24	loads 911 complex onto DNA; signaling role
mec3	sensor (part of 911 complex)
ddc1	sensor (part of 911 complex)
dun1	serine-threonine kinase
chk1	effector kinase

After transformation with *rad52::LEU2* DNA fragments as previously described, Leu^+ colonies were streak-purified and chromosomal DNA was extracted from several of them for each strain. The genomic DNAs were then tested by PCR with the test primers RAD52E and LEU2A as before. An example of PCR products that underwent agarose electrophoresis is shown in the figure below (Figure 24). The PCR products were run on a 0.7% agarose gel. As shown in the figure, *rad17 rad52* isolates 3 and 5, *dun1 rad52* isolate 1, *rad9 rad52* isolates 1, 3, and 4, and *mec3 rad52* isolate 2 produced 1200 bp bands, confirming proper integration of *LEU2* into *RAD52*.

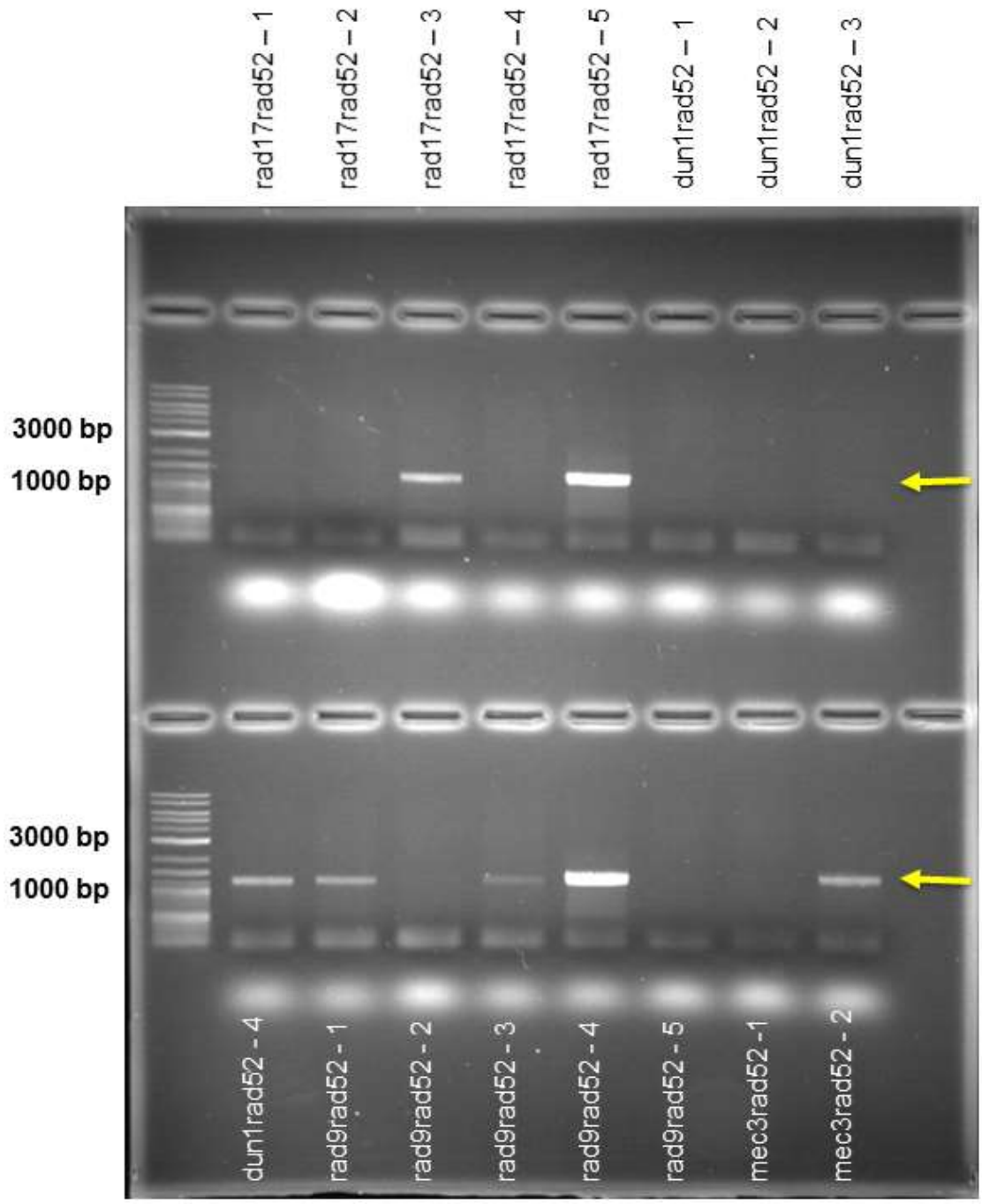

Figure 24. PCR products analyzed by agarose gel electrophoresis to confirm knockout of *RAD52*. The presence of a 1200 bp band indicates transformants that are *RAD52* deficient. Yellow arrows indicate the 1200 bp band.

Confirmed *rad52 ddr* double mutant isolates were inoculated into YPDA broth at $3x10^6$ cells/mL, grown to mid log phase at 30°C and levels of G_2/M cells quantified. G_2/M cells were reduced to WT levels in 5 of the *rad52* DNA damage checkpoint double mutants (with knockouts of *mec3, ddc1, rad9, rad17,* and *rad24*) and to near WT levels in 2 others (*dun1* and *chk1*) (Figure 25). These results demonstrate that the high G_2 phenotype observed in *rad52* cells is dependent on DNA damage checkpoint genes.

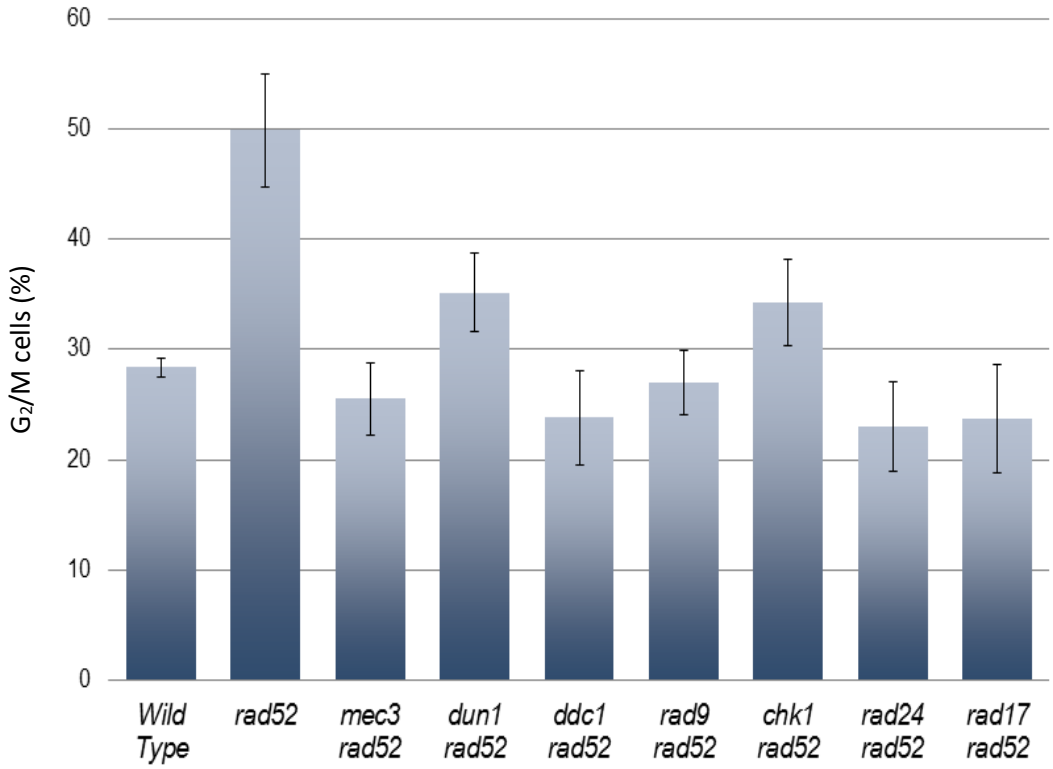

Figure 25. Quantification of the percentage of G_2/M cells in 7 different *rad52* checkpoint double mutants. Inactivation of the DNA damage checkpoint returned homologous recombination-deficient *rad52* cell cultures to near WT levels of G_2/M cells.

We hypothesized that DSB repair-deficient strains that were coupled with a checkpoint mutation might exhibit stress or slow growth effects when grown over many generations due to an accumulation of unrepaired DNA damage. The idea is that cells are progressing into M phase regularly with damaged chromosomes, which may be further damaged by the forces applied by the mitotic spindle in metaphase and anaphase. To test this hypothesis, four *rad52*$^{-}$ checkpoint^{-} double mutant strains (*rad9 rad52, rad17 rad52, rad24 rad52, chk1 rad52*) were created that contained a plasmid (pGAL::RAD52) expressing *RAD52* via a galactose-regulated promoter. This design allowed the expression of *RAD52* to be turned on and off depending on whether or not the growth media contained galactose or glucose (Figure 26).

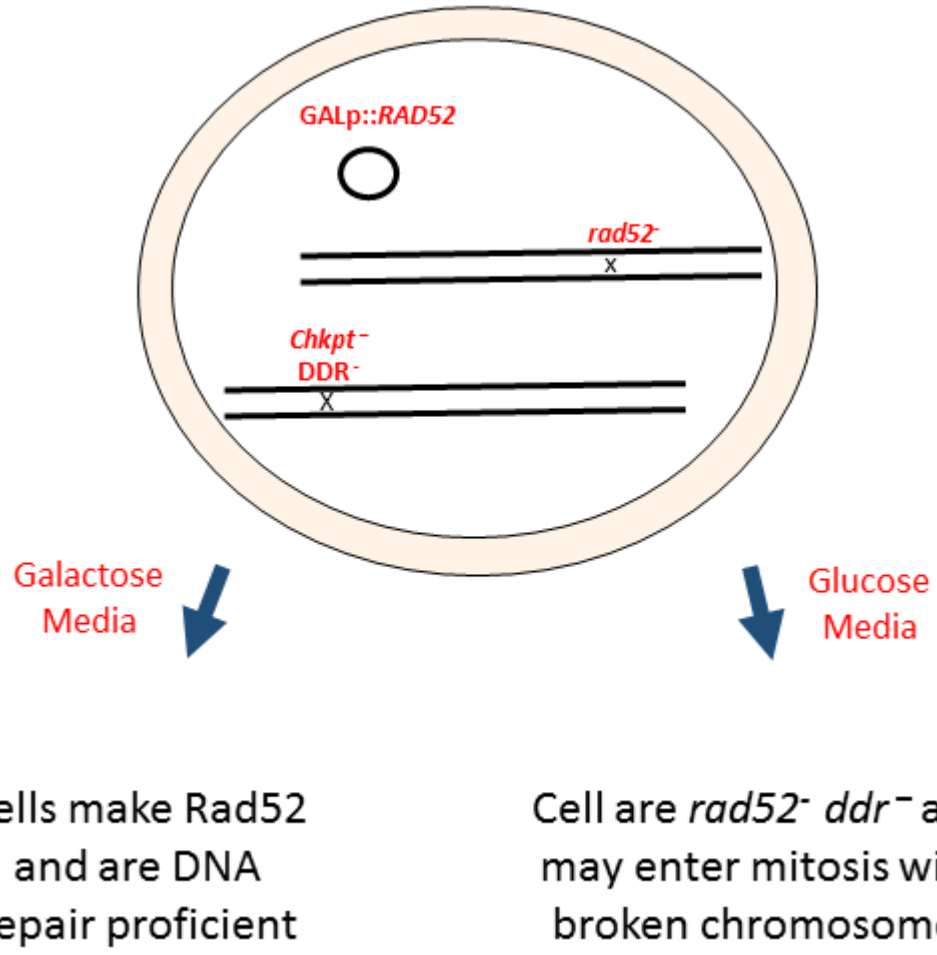

Figure 26. Design schematic of *rad52- ddr-* double mutants that were transformed with a plasmid expressing *RAD52*. Depending on the growth medium, cells will either be expressing Rad52 or not.

After being transformed with the pGAL::RAD52 plasmid, checkpoint mutant strains were transformed with the *RAD52::LEU2* plasmid fragment to inactivate the chromosomal copy of *RAD52* and spread onto galactose minus leucine and uracil plates. Colonies were PCR verified to ensure the fragment underwent recombination with the

correct locus on chromosome XIII, knocking out *RAD52* and replacing it with *LEU2* as described previously. Isolates were streak purified on galactose media that was deficient in uracil and leucine. The uracil deficiency selected for cells that contained the pGAL::RAD52 plasmid while galactose drove the expression of *RAD52* via the galactose promoter on the plasmid. The leucine deficiency selected for cells that have the *RAD52* locus disrupted with, and are actively expressing, the *LEU2* gene. When plated on plates containing 5-FOA, which is toxic to *URA3* cells, cells that had naturally lost the pGAL::RAD52 plasmid could be selected for and would grow to form colonies. This design allowed study of *rad52* checkpoint double mutant cells without the worry of accumulation of DNA damage over generations of growth before the study took place.

After constructing the new double mutants, we wanted to observe the effects on growth that being *rad52*-deficient and checkpoint-deficient had on these strains. Cells were repeatedly streaked to either galactose or glucose plates for a series of 6 streaks as shown below (Figure 27). In the left pathway, cells have an actively transcribed plasmid *RAD52* gene and are checkpoint-deficient only. In the right pathway, cells are *RAD52*-defective and checkpoint-defective, potentially causing them to pass through M phase repeatedly with unrepaired DNA damage. Each medium-sized colony on a plate has undergone ~21 generations or cell cycles, starting from a single cell.

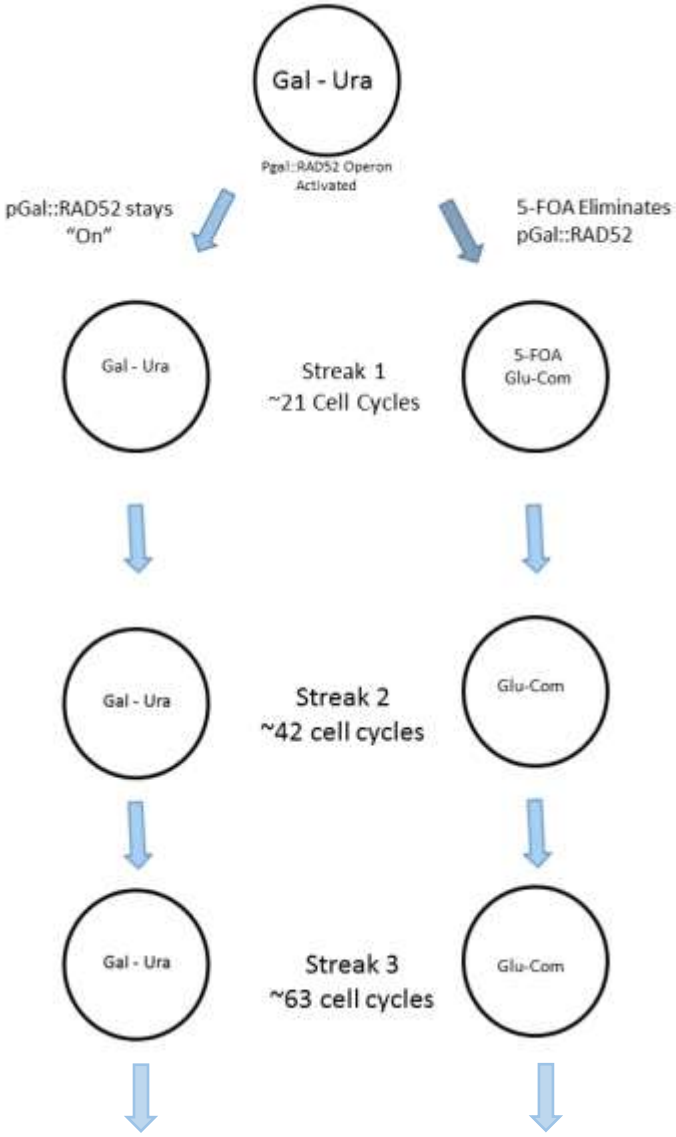

Figure 27. Diagram of the two pathways checkpoint *rad52 ddr* double mutants underwent during plate streaking assays. Colonies forming on earlier plates were picked and restreaked to new plates, forcing the cells to undergo many generations of growth with unrepaired chromosomes.

The four double mutant strains were streaked repeatedly, for a total of 6 streak plates, corresponding to ~126 generations, but growth rates and colony sizes did not change during the course of the experiment (data not shown). These results indicate that lack of *RAD52* and a functional DNA damage response does not affect viability strongly in most of the cells.

We observed that many *rad52* cells appeared to be enlarged compared to WT cells when analyzed using phase contrast microscopy. The next aim intended to quantify the large, distended phenotype observed in populations of *rad52* cells. Cells were grown for four hours at 30^{o}C to mid log phase as before prior to being analyzed and measured via phase contrast microscopy. Cell sizes across the largest diameter of the mother cell were measured using a micrometer scale provided by the Scope Image-Pro software package. A total of 150 WT and 150 *rad52* cells were analyzed. The average sizes of unbudded, small-budded and large-budded cells are depicted in Figure 28. These cell diameters were ~ 5.25, 5.25, and 5.75 µm in WT cells. In contrast to this, *rad52* cells in all three categories were larger with sizes of 6.1, 6, and 7.25 µm, respectively. This result indicates that unbudded and small-budded *rad52* cells are 16.2% and 14.3% larger than the equivalent types of WT cells. Large-budded (G_2/M) cells exhibited an even larger difference, with *rad52* cells 26.1% larger than the equivalent WT cells.

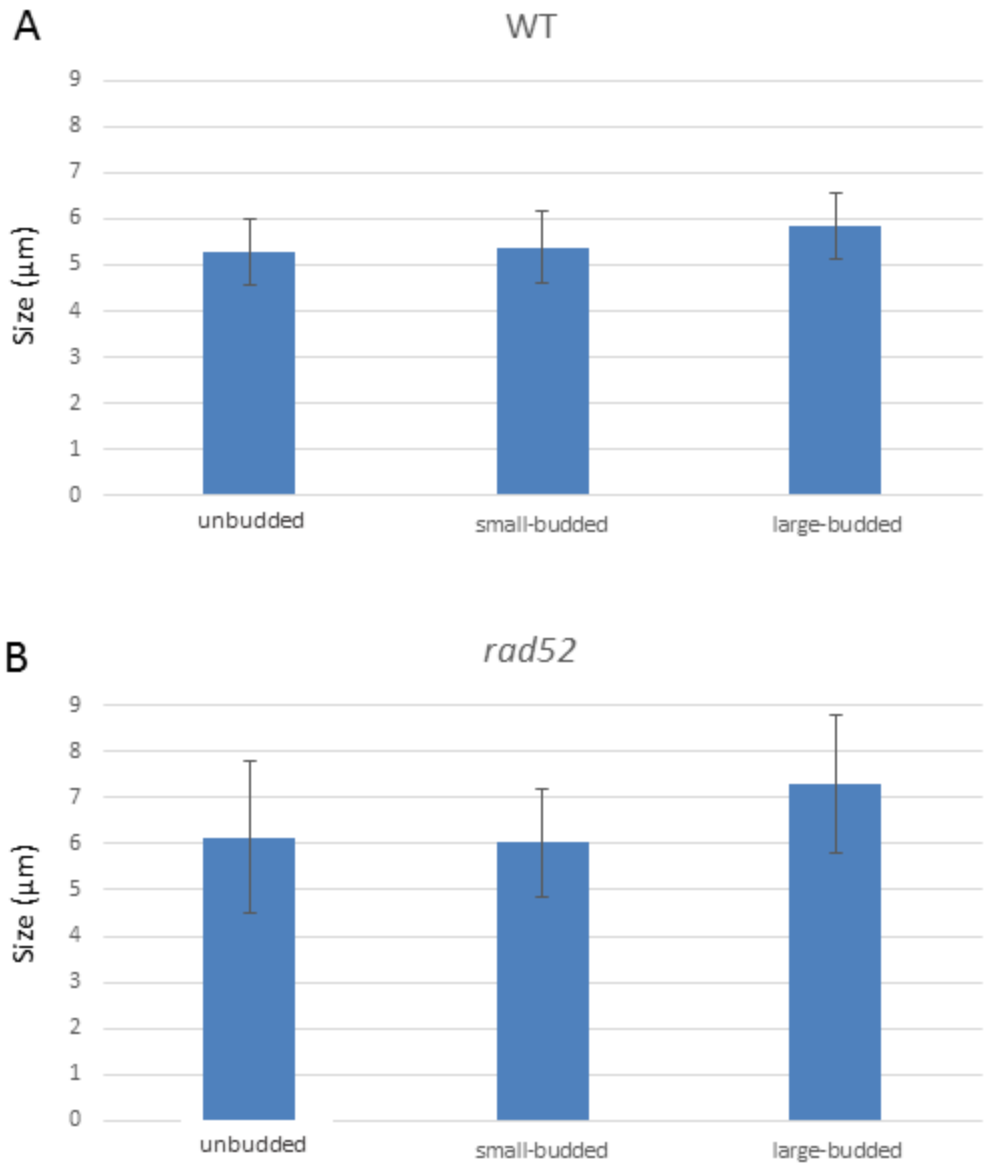

Figure 28. Unbudded, small-budded, and large-budded cell size averages after 4 hours of growth in YPDA at 30ºC for WT (A) and *rad52* cells (B).

Large-budded homologous recombination-deficient *rad52* cells were found to be, on average, 1.5 µm larger than WT cells of the same strain background. Average sizes were 5.8 µm and 7.3 µm for WT and *rad52* cells, respectively (Figure 29, dashed line). Figure 28 shows the distribution of sizes among WT and *rad52* cells. All WT cells were between 4 and 8 µm, with a relatively narrow distribution (blue line). In contrast, *rad52* cells ranged from 4 to 10 µm in size (red line), indicating much greater heterogeneity in size. The plot distribution seen in Figure 29 was generated in excel. Four column headers were made: Data, Distribution, Average, and Standard Distribution in columns A-D. Data was sorted in column A from lowest to highest using the sort command. The average and the standard deviation of the data set were found by entering excel formulas into cell C2 and D2, =AVERAGE(A2:AX) and =STDDEV(A2:AX). Next, The distribution of each data point was found by entering the following formula into cell B2: = NORMDIST(A2,C2,D2,FALSE). The formula was then dragged down the B column labelled Distribution beside every data point in the "Data" A column. The data and distribution columns were then selected and a scatter plot was formed from the selected cells.

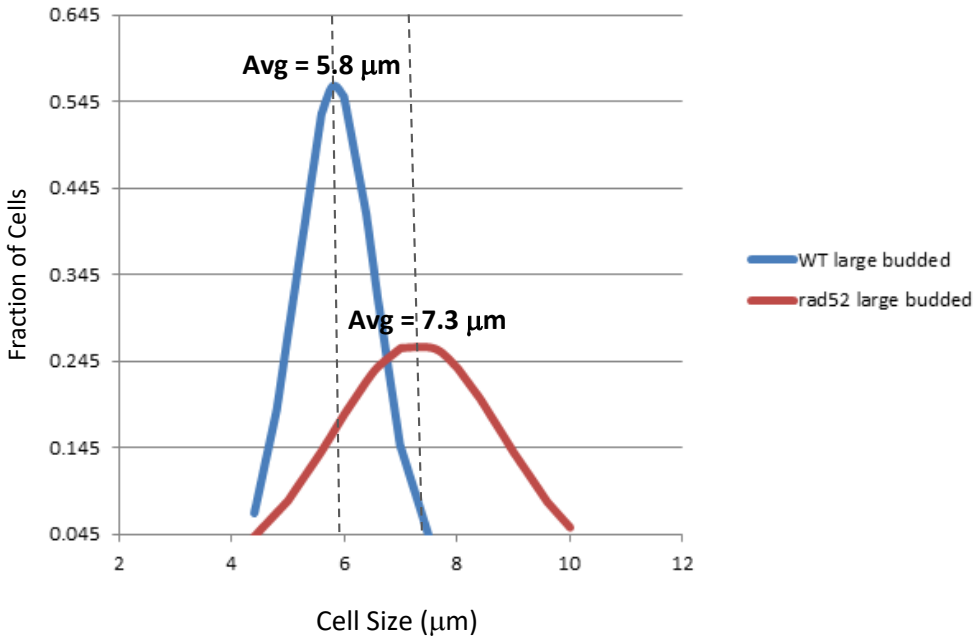

Figure 29. Cell size distributions for WT (blue) and *rad52* (red) large-budded cells. Homologous recombination-deficient *rad52* cells were on average ~1.5 µm larger than WT cells of the same strain background. Dashed lines indicate average sizes of WT and *rad52* cells, which were 5.8 and 7.3 µm, respectively.

To gain a better perspective of the distribution on cell sizes for large-budded WT and *rad52* cells, the cells were broken down into three size categories, 4.0 – 5.9 µm, 6.0 – 7.9 µm, and ≥ 8 µm (Figure 30). WT cultures had no cells that fell into the ≥ 8.0 µM category, whereas almost 50% of *rad52* cells were ≥ 8.0 µM. Interestingly, only 50% of the large-budded *rad52* cells were ≥ 8.0 µM and the remaining 50% were the same size as WT cells. If cell enlargement is a response to elevated levels of unrepaired DNA damage, this result implies that only about half of the large-budded *rad52* cells have unrepaired damage above the threshold for inducing a cellular response.

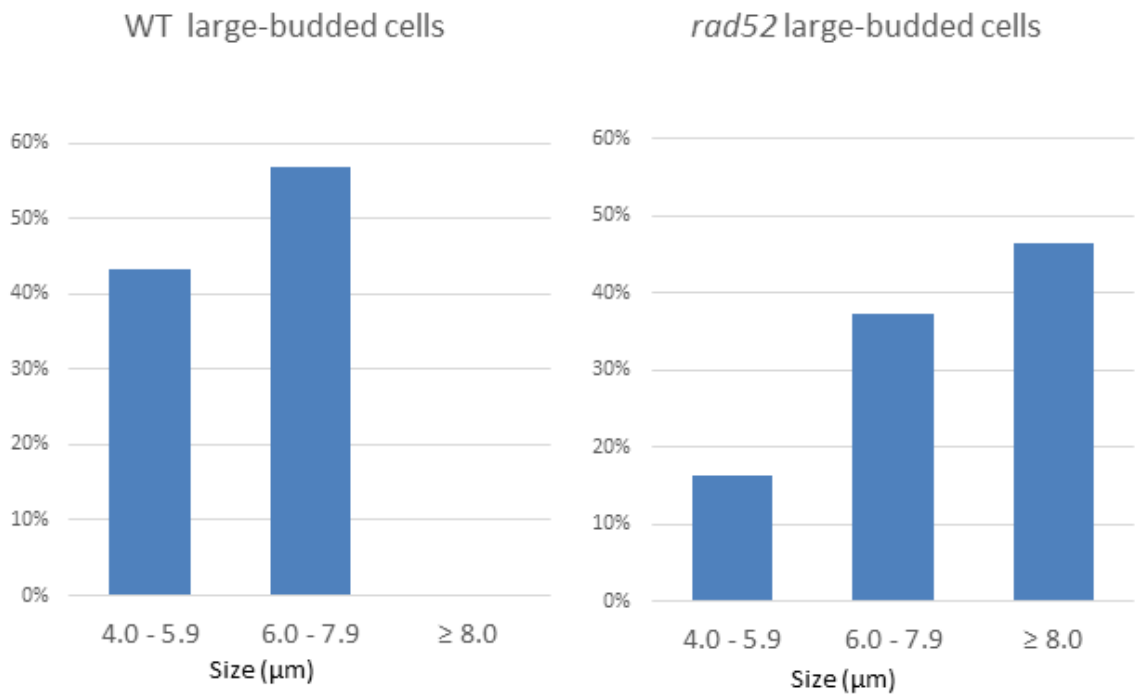

Figure 30. Size distributions of large budded homologous recombination-deficient *rad52* cells vs. WT cells of the same strain background. Cells were broken down into the following size categories: 4.0-5.9, 6.0-7.9, ≥ 8.0 µm. WT cultures had no cells that fell into the ≥ 8.0 µm category, whereas almost 50% of *rad52* cells were ≥ 8.0 µm. One hundred and fifty cells were analyzed for both *rad52* and WT cultures.

The previous experiments revealed that *rad52* cell cultures have high levels of large-budded cells. Cells' nuclear morphologies and their proportion of G_2 phase vs M phase cells were investigated next. The difference between G_2 and M cannot be observed by phase contrast microscopy, but instead has to be visualized with a nuclear stain such as DAPI (4',6-diamidino-2-phenylindole). DAPI is a blue fluorescent stain that binds

strongly to AT-rich regions of DNA via minor groove binding. It is a planar conjugated molecule excited by light of ~400 nm wavelength (48).

Both WT and *rad52* BY4742 cells were grown for four hours so they would be in logarithmic phase growth before being sonicated and formaldehyde-fixed for two hours to preserve nuclear morphologies. After being rehydrated with 70% ethanol for an hour, nuclei were stained with DAPI and treated with ProLong Gold Antifade mountant to prevent the fluorescent signal from photobleaching. After a 24 hour dark fixation period, cells were analyzed microscopically to compare WT and *rad52* cells' nuclear morphologies. In the seminal paper by Weinert and Hartwell (43), treatment with X-rays or UV light caused an increase in large-budded G_2 cells with a medial nuclear division (mND) morphology. Large-budded cells were classified into two distinct groups, mND (medial nuclear division morphology) and M (mitosis). Cells at the mND stage of G_2 exhibit three possible nuclear structures whereby the nucleus is found near or across the neck of the bud (Figure 31).

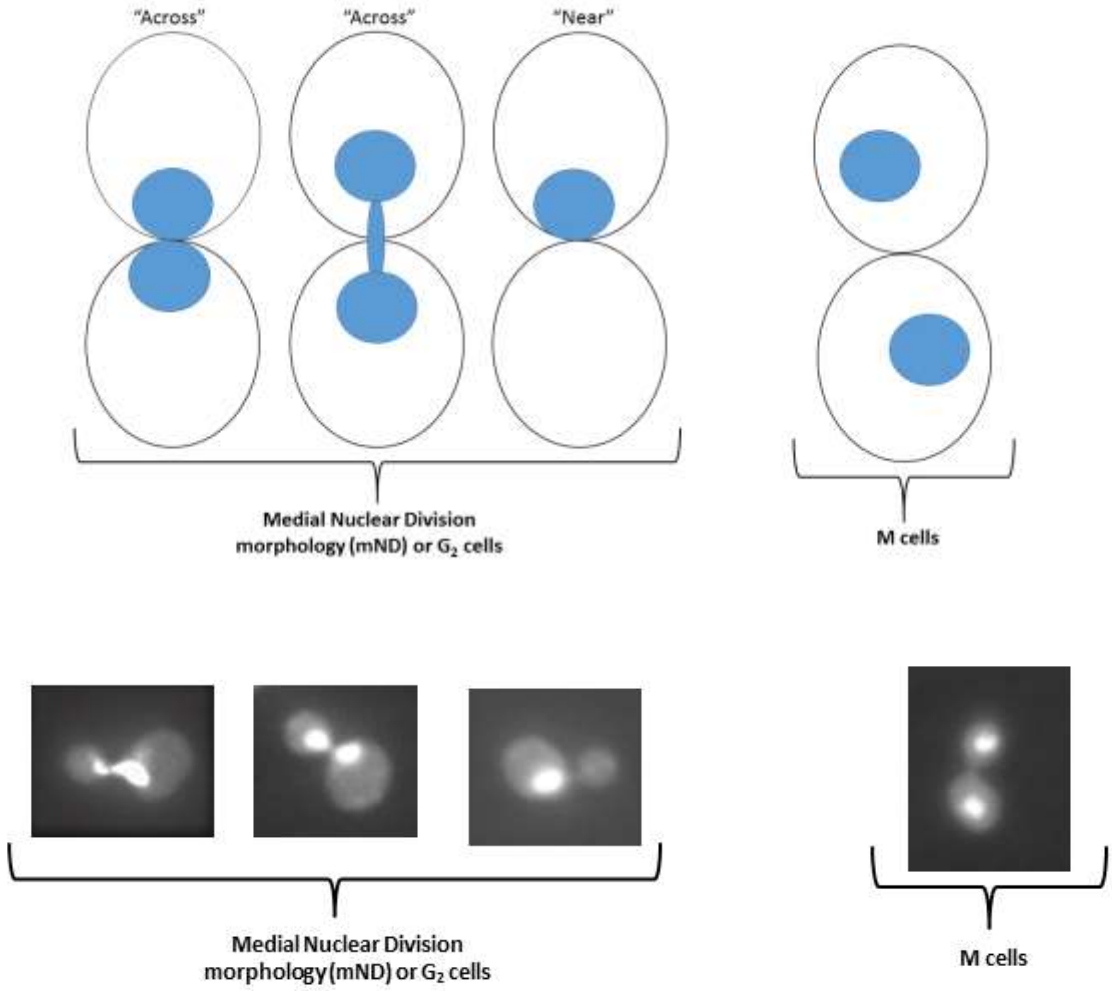

Figure 31. Classification of large-budded cells as mND or M cells based on observed nuclear morphologies using DAPI staining. Cartoon example (top) actual DAPI stained cells (bottom) from the current project.

Each imaged field of cells was first analyzed to report on the total number of cells in each field. Example of fields are shown below (Figure 32).

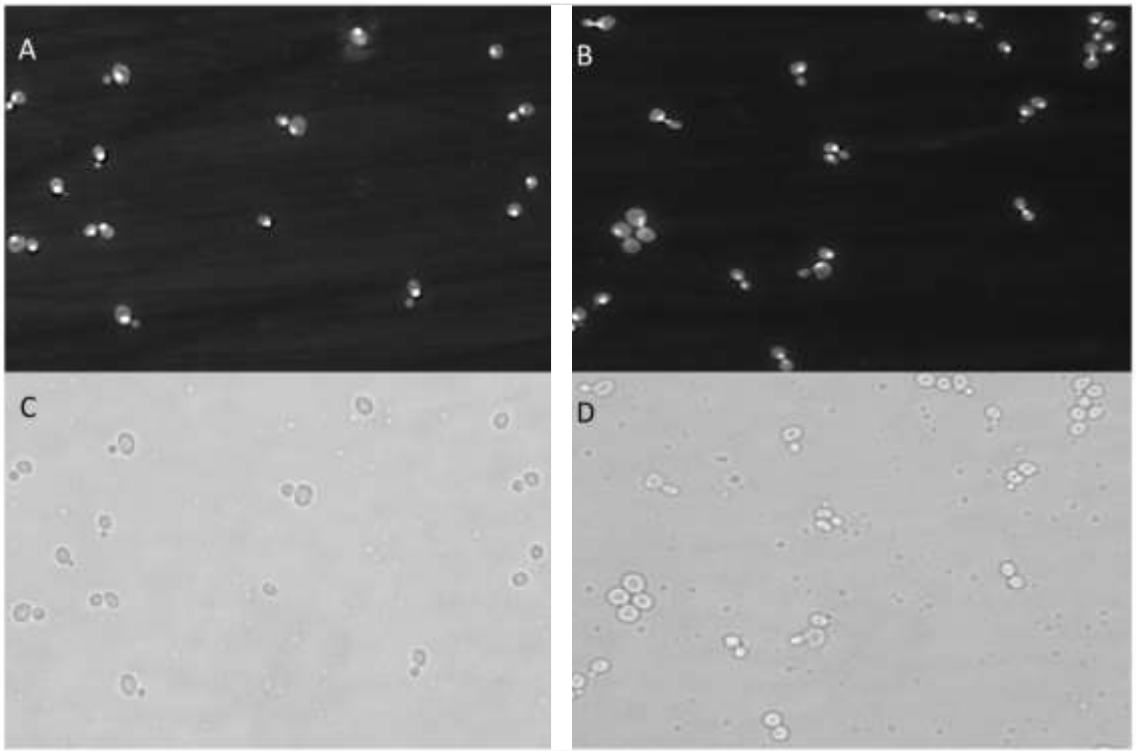

Figure 32. Example of DAPI and transmitted images of WT and *rad52* cells. A and B are the DAPI-stained images of WT and *rad52* cells, respectively. C and D are the same fields imaged with transmitted light.

All large-budded cells were identified using both the transmitted and DAPI stained images of each field. Nuclear morphologies were then determined and quantified and results are summarized in Table 8. Over 90% of the large-budded *rad52* cells exhibited an mND phenotype. These experiments demonstrated that the nuclear structures found in most large-budded *rad52* cells were consistent with the findings of past studies on X ray- and ultraviolet light-induced G_2 arrest of yeast cells (43).

Table 8. Summary of DAPI staining analysis of *rad52* and WT cells.

	# of fields	Total cells analyzed	Total large-budded cells	Average large-budded cells/field	Average M cells/field	Average mND cells/field	mND cells among large-budded cells
WT	21	298	143	6.5	1.6	4.9	75.4 %
rad52	10	297	152	11.7	0.7	11.0	94.0 %

IV. SUMMARY AND CONCLUSIONS

The primary focus of this project was to investigate the observation that mutant yeast cells defective in DNA double-strand break repair have a larger percentage of G_2 cells in liquid cultures than wild type cells. This indicates that these cells are spending more time in G_2 phase. Previous work suggested that *rad52* and *rad51* cells, both defective in DSB repair, have a higher number of G_2 cells than wild type cells (43, 46). These mutants have the same phenotype that normal, healthy cells have after being exposed to DNA damaging agents. We concluded that these DSB repair-deficient cells pause in G_2 phase due to the inability to repair endogenous DNA damage. We speculate that a major source of this damage is caused by Reactive Oxygen Species (ROS) which are a normal, unavoidable byproduct of oxygen metabolism. The unrepaired damage then results in a constitutively activated DNA damage response. This project successfully quantitated the changes in cell morphology and cell cycling in *S. cerevisiae* mutants that are deficient in DNA double-strand break repair via the HR pathway as well as cells that are deficient in both DSB repair and DNA damage checkpoint response.

The first objective of this project was to reproduce Paige Hall's findings that *rad52* cells have a higher number of G_2 cells than WT cells. It was re-analyzed and observed that WT cell cultures had about 28% G_2/M cells while *rad52* cells had 50% G_2/M cells. These results were consistent with her previous findings.

Cell cycle doubling times were calculated for WT and *rad52* cells during logarithmic phase growth. *rad52* mutants had doubling times that were 50% longer than WT cells (128 minutes as compared to 83 minutes). Total cell cycling time (doubling

time) and the percentages of cells in G_1 (unbudded), S (small-budded), and G_2 /M (large-budded) during logarithmic phase growth were multiplied to calculate the minutes spent in each phase. *rad52* cells spent 2.7 fold more time in G_2 phase than WT cells (63.8 minutes as compared to 23.5 minutes). In contrast minutes spent in G_1 and S were similar in the two strains.

How the percentage of G_2/M cells changes as cells transition from stationary phase, through logarithmic phase, and back to stationary phase growth was investigated. The percentage of large-budded cells continued to increase in *rad52* cells until hour 8 where they reached 67%, but WT cells reached a peak of 34% at hour 4.

The possibility that inactivation of other members of the RAD52 epistasis group might also lead to high levels of G_2 cells was also examined. *rad51, rad54, rad55, rad57,* and *rad59* mutants also exhibited higher percentages of G_2 cells than WT cells, with non-overlapping standard deviation error bars. *rdh54* mutants were the only cells that did not exhibit a strong increase in G_2 cells. Rdh54 plays a role in homologous recombination in diploid cells and during meiosis (44). Neither haploid nor diploid *rdh54* strains exhibited high G_2 cells, suggesting that high levels of unrepaired DNA lesions are not present when this repair protein is absent.

Time spent in in G_1, S, and G_2 phase was investigated for RAD52 epistasis group mutants. All mutants displayed elevated doubling times (~90 minutes as compared to ~83 min for WT cells). *rad52* cells were different from the others and exhibited a much longer doubling time of 128 minutes.

The length of time RAD52 epistasis group members were spending in each phase of the cell cycle was calculated as done previously for *rad52* cells. WT cells spent 24 minutes in G_2 phase, *rad51*, *rad54*, *rad55*, *rad57*, and *rad59* cells spent nearly twice as long in G_2 (between 39.2 and 46.0 minutes).

Experiments with the *MATα* mutants showed that *rad52* mutant phenotypes were much more extreme than in the other DSB repair mutants (e.g., 128 minute doubling time versus ~90 min for other mutants). New experiments were performed to see if this extreme phenotype that *rad52* mutants exhibit would also be observed in BY4741 *MATa rad52* mutants. As seen previously in BY4742 cells, the BY4741 *rad52* mutants had a more extreme phenotype than *rad51* cells, with a doubling time of 115 minutes versus 85 minutes. Doubling times were multiplied by the percent of G_2 cells present during logarithmic phase growth to obtain an estimate of the average time cells were spending in G_2 phase. BY4741 *rad52* cells spent ~2.5 times the amount of time that WT cells spend in G_2. This is comparable to the ~2.7 times the amount of time BY4742 *rad52* cells spend in G_2 phase as compared to WT. These experiments demonstrate that DSB repair-deficient *rad51* and *rad52* mutants exhibit high G_2 cells in both *MATa* and *MATα* strains. They also confirm that *rad52* cell phenotypes are more extreme than those seen in *rad51* cells in both cell types.

To test our hypothesis that *rad52* mutants have high levels of G_2/M cells due to unrepaired DNA damage and thus a constitutively activated cell cycle checkpoint response, new double mutants were created. The strains created by this procedure were *rad52 rad9*, *rad52 rad17*, *rad52 rad24*, *rad52 mec3*, *rad52 ddc1*, *rad52 dun1* and *rad52 chk1* double mutants. G_2/M cells were reduced to WT levels in 5 of the *rad52* DNA

damage checkpoint double mutants and to near WT levels in 2 others. These results demonstrate that the high G_2 phenotype observed in *rad52* cells is dependent on DNA damage checkpoint genes.

We hypothesized that DSB repair-deficient strains that were coupled with a checkpoint mutation might exhibit stress or slow growth effects when grown over many generations due to an accumulation of unrepaired DNA damage. To test this hypothesis, four *rad52*$^-$ checkpoint$^-$ double mutant strains (*rad9 rad52*, *rad17 rad52*, *rad24 rad52*, *chk1 rad52*) were created that contained a plasmid (pGAL::RAD52) expressing *RAD52* via a galactose-regulated promoter. This design allowed the expression of *RAD52* to be turned on and off depending on whether or not the growth media contained galactose or glucose (Figure 26). The 4 double mutant strains were streaked repeatedly, for a total of 6 streak plates, corresponding to ~126 generations, but growth rates and colony sizes did not change during the course of the experiment (data not shown). These results indicate that lack of *RAD52* and a functional DNA damage response does not affect viability strongly in most of the cells.

The next aim intended to quantify the large, distended phenotype observed in populations of *rad52* cells. Homologous recombination-deficient *rad52* cells were on average 1.5 μm larger than WT cells of the same strain background. All WT cells were between 4 and 8 μm but *rad52* cells ranged from 4 to 10 μm in size, indicating much greater heterogeneity in size.

The distribution of cell sizes for large-budded WT and *rad52* cells were broken down into size categories, 4.0 – 5.9 μm, 6.0 – 7.9 μm, and ≥ 8 μm. WT cultures had no cells that fell into the ≥ 8.0 μm category, whereas almost 50% of *rad52* cells were ≥ 8.0

μm. Thus 50% of the large-budded *rad52* cells were ≥ 8.0 μm and the remaining 50% were the same size as WT cells. If cell enlargement is a response to elevated levels of unrepaired DNA damage, this result implies that only about half of the large-budded *rad52* cells have excessive levels of unrepaired damage.

DAPI (4',6-diamidino-2-phenylindole) staining was used to differentiate between M and G_2 cells in logarithmic phase WT and *rad52* cultures. Large-budded cells were classified into two groups, mND (medial nuclear division morphology) and M (mitosis). mND cells were identified by three possible nuclear structures whereby the nucleus is found near or across the neck of the bud. These experiments revealed that 95% of the large-budded *rad52* cells exhibited the mND phenotype. Thus, the vast majority of the large-budded cells in log phase *rad52* cell cultures are in G_2 phase, not M phase. Half of these G_2 cells are enlarged with a distended phenotype. These observations in *rad52* cultures were consistent with the findings of past studies on X ray- and ultraviolet light-induced G_2 arrest of yeast cells (43).

These experiments lead us to speculate that WT yeast cells are exhibiting a basal level of DNA damage checkpoints that are constitutively activated. We believe the main antagonist of this activation is aerobic metabolism and the natural production of ROS. Instead of taking a set amount of time, G_2 phase could innately consist of a growth phase with an additional varied amount of time for DNA damage repair based on the intensity of DDR signal received from the cell.

Further experiments include growing WT BY4742 cells in YPDA broth in the presence of a strong antioxidant such as N-acetylcysteine. If cells spend less time in G_2 phase than the normal ~24.5 minutes, this could indicate that the ROS species that are a

normal part of aerobic metabolism are influencing the magnitude of checkpoint activation based on DDR response. Thus, the pause in G_2 due to DDR checkpoint response could be thought of as an adjustable response instead of an outcome that is on or off.

Humans and other higher level eukaryotes defective in DNA repair may also be exhibiting a constitutive activation of DNA damage checkpoints. Humans that are deficient in their main DSB repair pathway, NHEJ, may have a measurable G_2/M checkpoint similar to yeast.

REFERENCES

1. Lewis, L.K.; Karthikeyan, G.; Cassiano, J.; Resnick, M.A. Nucleic Acids Res. **2005**, 33, 4928-4939.

2. Lewis, L.K.; Resnick M.A. Mutat. Res. **2000**, 451, 71-89.

3. Lewis, L.K.; Westmoreland, J.W.; Resnick, M.A. Genetics **1999**, 152, 1513-1529.

4. Ciccia, A.; Elledge, S. J. Mol. Cell **2010**, 40, 179–204.

5. Perrone, G. G.; Tan, S.-X.; Dawes, I. W. *Biochim. Biophys. Acta - Mol. Cell Res.* **2008**, 1783, 1354–1368.

6. Lewis, L.K.; Kirchner, J.M.; Resnick, M.A. Mol. Cell Biol. **1998**, 18, 1891-1902.

7. Lewis, L.K.; Karthikeyan, G.; Westmoreland, J.W.; Resnick, M.A. Genetics **2002**, 160, 49-62.

8. Hefferin, M.; Tomkinson, A. DNA Repair **2005**, 4, 639-648.

9. Williams, R.S.; Trainer, J.A. Mol. Cell **2007**, 25, 789-791.

10. Daley, J.M.; Palmbos, P.L.; Wu, D.; Wilson, T.E. Annu. Rev. Genet. **2005**, 39, 431-451.

11. Symington, L.S. Microbiol. Mol. Bio. Rev. **2002**, 66, 630-670.

12. Wyman, C; Kanaar, R. Annu. Rev. Genet. **2006**, 40, 363-383.

13. Lisby, M.; Mortensen, U.H.; Rothstein, R. Nat. Cell Biol. **2003**, 5, 572-577.

14. Shim, E.Y.; Ma, J.L.; Oum, J.H.; Yanez, Y.; Lee, S.E. Mol. Cell Biol. **2005**, 25, 3934-3944.

15. Unal, E.; Heidinger-Pauli, J.M.; Koshland, D. Science **2007**, 317, 245-248.

16. Unal, E.; Arbel-Eden, A.; Sattler, U.; Shroff, R.; Lichten, M.; Haber, J.E.; Koshland, D. Mol. Cell **2004**, 16, 991-1002.

17. Strom, L.; Karlsson, C.; Betts Lindroos, H.; Wedahl, S.; Katou, Y.; Shirahige, K.; Sjogren, C. Science **2007**, 317, 242-245.

18. Kim, J.; Krasieva, T.B.; LaMorte, V.; Taylor, A.M.; Yokomori, K. J. Biol. Chem. **2002**, 277, 45149-45153.

19. Nakada, D.; Hirano, Y.; Sugimoto, K. Mol. Cell Biol. **2004**, 24, 10016-10025.

20. Grenon, M.; Magill, C.P.; Lowndes, N.F.; Jackson, S.P. FEMS Yeast Res. **2006**, 6, 836-847.

21. Heikkinen, K.; Rapakko, K.; Karppinen, S.M.; Erkko, H.; Knuutila, S.; Lundan, T.; Mannermaa, A.; Borresen-Dale, A.L.; Borg, A.; Barkardottir, R.B.; Petrini, J. Winqvist, R. Carcinogenesis **2006**, 27, 1593-1599.

22. Gullo, C.; Au, M.; Feng, G.; Teoh, G. Biochem. Biophys. Acta. **2006**, 1765, 223-234.

23. Ramotar, D.; Wang, H. Curr. Genet. **2003**, 43, 213-224.

24. Chang, M.; Bellaoui, M.; Boone, C.; Brown, G. PNAS **2002**, 99, 16934-16939.

25. Allison, D.P.; Kerper, P.S.; Doktycz, M.J.; Spain, J.A.; Modrich, P.; Larimer, F.W.; Thundat, T.; Warmack, R.J. Proc. Natl. Acad. Sci. **1996**, 9, 8826-8829.

26. Windolph, S.; Fritz, A.; Oelgeschlager, T.; Wolfes, H.; Alves, J. Biochem. **1997**, 36, 9478-9485.

27. Pingoud, A.; Fuxreiter, M.; Pingoud, V.; Wende, W. Cell Mol. Life Sci. **2005**, 62 (6) 685-707.

28. Pingoud, A.; Jeltsch, A. Nucleic Acids Res. **2001**, 29, 3705-3727.

29. Barnes, G.; Rine, J. Proc. Natl. Acad. Sci. **1985**, 82, 1354-1358.

30. Sherman, F. *Methods Enzymol.* **2002**, *350*, 3–41.

31. Hefferin, M. L.; Tomkinson, A. E. DNA Repair (Amst). **2005**, 4 (6), 639–648.

32. Feng, Q.; Düring, L.; de Mayolo, A. A.; Lettier, G.; Lisby, M.; Erdeniz, N.; Mortensen, U. H.; Rothstein, R. DNA Repair (Amst). **2007**, 6 (1), 27–37.

33. Grenon, M.; Gilbert, C.; Lowndes, N. F. Nat. Cell Biol. **2001**, 3 (9), 844–847.

34. Wilbur; Molecular Biology of the Gene, Pearson: New York, **2014**

35. Summers, J. A. *Application of a Novel Endonuclease Sensitivity Assay to Identify New Genes that Affect DNA Repair and Chromosome Stability*. M.S. Thesis, Texas State University, San Marcos, TX, **2008**

36. Nguyen T. *Investigation of DNA stability in Saccharomyces cerevisiae metants defective in the repair of broken chromosomes*. M.S. Thesis, Texas State University, San Marcos, TX, **2012**

37. Kumar, R.; Cheok, C. F. DNA Repair **2014**, 15, 54–59.

38. Matsuzaki, K.; Shinohara, A.; Shinohara, M. Genetics **2008**, 179 (1), 213–225.

39. King, M.-C. Science **2003**, 302 (5645), 643–646.

40. Venkitaraman, A. R. Cell **2002**, 108 (2), 171–182.

41. Sambrook, J. Molecular Cloning: A Laboratory Manual, 4th ed.; Cold Spring Harbor Laboratory Press, **2012**.

42. Downs, J. A.; Jackson, S. P., A means to a DNA end: the many roles of Ku. Nat Rev Mol Cell Biol **2004**, 5 (5), 367-78.

43. Weinert and L. H. Hartwell, Science **1988**, 241:317-322

44. Cortes-Ledesma F, et al. Nucleic Acids Res **2007,** 35(19):6560-70

45. Fingerhut, R.; Kiefer, J.; Otto, F. MGG Molecular & General Genetics **1984**, 193 (1), 192–194.

46. J. Summers, "Assay to Identify New Genes that Affect DNA Repair and Chromosome Stability". Masters Thesis, Texas State University, **2008**

47. Schmidt, K. H.; Kolodner, R. D. Molecular and Cellular Biology **2004**, 24 (8), 3213–3226

48. Tanious, F. A.; Veal, J. M.; Buczak, H.; Ratmeyer, L. S.; Wilson, W. D. Biochemistry **1992**, 31 (12), 3103–3112.

49. Christianson, T. W.; Sikorski, R. S.; Dante, M.; Shero, J. H.; Hieter, P. Gene **1992**, 110 (1), 119–122.

50. Nugent CI, Bosco G, Ross L, Evans SK, Salinger AP, Moore JK, Haber J, Lundblad V: Curr Biol **1998**, 8:657-660

51. Carbone A, Fioretti F, Fucci L **2012**, 59,275-278.

52. Lee, C. K.; Araki, N.; Sowersby, D. S.; Lewis, L. K. Yeast **2011**, 29 (2), 73–80.

53. Larionov,V. Nucleic Acids Res. **1994** (22),4154-4162.

54. Morrison,A. EMBO J. **1993** (12), 1467-1473.

55. White, C. EMBO J. **1990** (9), 663-673.

56. Sikorski, R. S. Genetics. **1989** 122(1), 19-27

57. Brachmann, C. B. Yeast. **1998** 14(2):115-32.